Pergamon

Mineral surface catalysis of reactions between Fe^{II} and oxime carbamate pesticides

TIMOTHY J. STRATHMANN* and ALAN T. STONE

Department of Geography and Environmental Engineering, Johns Hopkins University, Baltimore, MD 21218, USA

Abstract—This study examines the reduction of oxime carbamate pesticides (oxamyl, methomyl, and aldicarb) by Fe^{II} in aqueous suspensions containing twelve different (hydr)oxide and aluminosilicate minerals. In the absence of Fe^{II}, mineral surfaces have no apparent effect on the pathways or rates of oxime carbamate degradation. In anoxic suspensions containing Fe^{II} and mineral surfaces, rates of oxime carbamate reduction are significantly faster than in equivalent mineral-free homogeneous solutions. Rates increase with increasing surface area loading (mineral surface area per volume of suspension) and pH. Kinetic trends are interpreted in terms of changes in Fe^{II} speciation. Quantitative modeling indicates a first-order dependence on total adsorbed Fe^{II} concentration and no significant dependence on adsorbed oxime carbamate concentration. Bimolecular rate constants describing the reactivity of adsorbed Fe^{II} with dissolved oxamyl decrease in the following order: silicon dioxide #2 > silicon dioxide #1 ≫ hematite #2 > titanium dioxide #1 > hematite #1 > titanium dioxide #2 > silicon dioxide #3 > aluminum oxide > kaolinite #1 > kaolinite #2 > goethite ≫ titanium dioxide #3. Possible factors responsible for the increased reactivity of adsorbed Fe^{II}, as well as for the relative reactivity of Fe^{II} adsorbed on different surfaces, are discussed. Results from this study demonstrate that mineral surfaces present in subsurface environments can substantially catalyze the reduction of oxime carbamate pesticides by Fe^{II}. Overall rates of pesticide degradation may be under predicted by > 1 order of magnitude if the effects of mineral surfaces are not accounted for. *Copyright © 2003 Elsevier Science Ltd*

1. INTRODUCTION

The reductive transformation of agrochemicals and related synthetic organic compounds in subsurface environments has been of increased interest in recent years. Soils, sediments and aquifers are often found to be oxygen deficient (Hering and Stumm, 1990; Postma et al., 1991). Reducing agents that are scarce in oxic environments (e.g., Fe^{II}, reduced sulfur compounds, reduced organic matter, obligate anaerobes) are often found to be abundant in anoxic and suboxic settings (Lovley and Phillips, 1988; Hering and Stumm, 1990; Postma et al., 1991; Stone et al., 1994; Rügge et al., 1998). As a result, pathways and kinetics of agrochemical transformations in reducing environments are often quite different from those observed in oxygenated environments (Larson and Weber, 1994).

Most laboratory and field studies examining the degradation of synthetic organic compounds in anoxic or suboxic environmental settings have not attempted to identify the specific reagents responsible for observed degradation (Tomizawa, 1975; Walters-Echols and Lichtenstein, 1977; Hale et al., 1991; Peijnenburg et al., 1992). Recently, however, several studies have attributed organic compound transformations in these settings to reduction by dissolved and particulate-bound Fe^{II} (Heijman et al., 1993, 1995; Rügge et al., 1998). Laboratory studies have found that a variety of organic compounds, most notably nitrobenzenes and halogenated methanes, are reduced by Fe^{II} (Wade and Castro, 1973; Schwarzenbach et al., 1990; Klausen et al., 1995; Erbs et al., 1999; Amonette et al., 2000; Cervini-Silva et al., 2000; Schultz and Gundl, 2000; Pecher et

al., 2002). Surprisingly, little attention has been given to the reduction of broader classes of agrochemicals.

The reactivity of Fe^{II} has been found to be heavily dependent on its speciation (Stumm and Lee, 1961; Tamura et al., 1976; Millero et al., 1991; Klausen et al., 1995; Cui and Eriksen, 1996; Park et al., 1997; Buerge and Hug, 1998, 1999; King, 1998; Liger et al., 1999; Schultz and Gundl, 2000). Several studies have demonstrated that natural and synthetic mineral surfaces act as catalysts for reactions involving Fe^{II} (Tamura et al., 1980; Klausen et al., 1995; Cui and Eriksen, 1996; Buerge and Hug, 1999; Liger et al., 1999; Amonette et al., 2000; Schultz and Gundl, 2000; Vikesland and Valentine, 2002; Pecher et al., 2002). For example, Pecher et al. (2002) reported that polyhalogenated methanes are unreactive with Fe^{II} in homogeneous solutions, but are rapidly reduced by Fe^{II} in aqueous suspensions of iron oxides. The degree of surface catalysis observed for various reactions has been reported to depend on a range of factors, including the identity of the mineral phase (e.g., goethite vs. lepidocrocite), mineral surface area, pH, and most notably the concentration and speciation of Fe^{II} adsorbed on mineral surfaces. Mineral surfaces may exert a similar catalytic effect on the reduction of widely used agrochemicals.

This study examines the influence of mineral surfaces on the reactivity of Fe^{II} with three structurally related oxime carbamate pesticides (OCPs; Fig. 1). Prior studies in this series have examined the degradation of oxamyl and related OCPs in homogeneous solutions containing Fe^{II}, and the influence of Fe^{II}-complexing inorganic and organic ligands on reaction kinetics (Strathmann and Stone, 2001, 2002a, 2002b).

Figure 2 illustrates the observed pathways for oxamyl degradation in Fe^{II}-containing solutions (Bromilow et al., 1986; Strathmann and Stone, 2001). An Fe^{II}-independent E1cb elimination reaction results in the formation of an oxime product

* Author to whom correspondence should be addressed, at the Department of Civil and Environmental Engineering, University of Illinois, Newmark Civil Engineering Laboratory, 205 North Mathews Avenue, Urbana, IL 61801, USA (strthmnn@uiuc.edu).
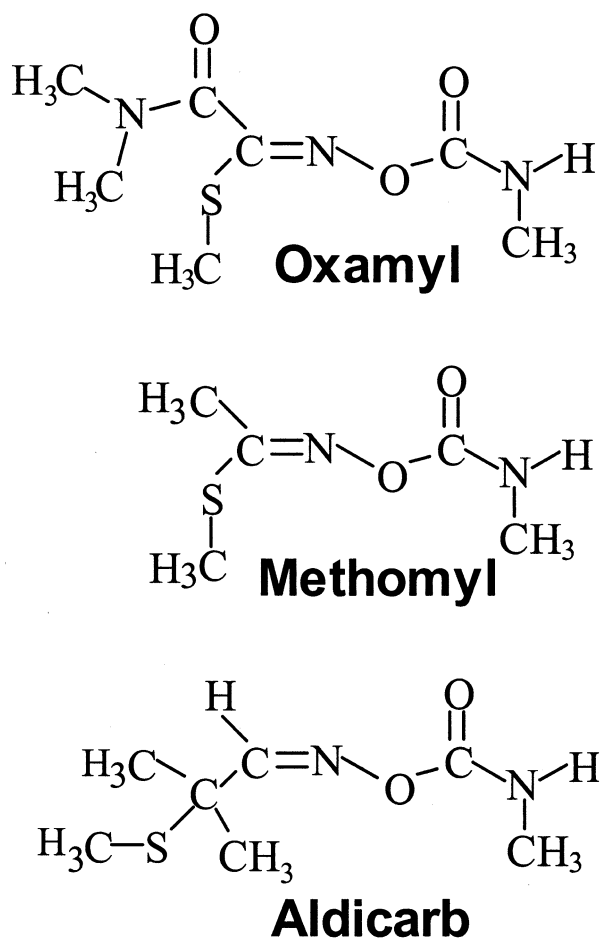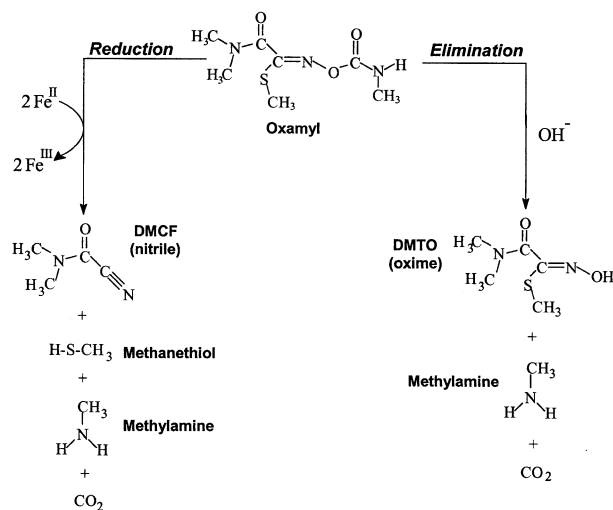
Fig. 1. Oxime carbamate pesticides.

Fig. 2. Observed pathways for abiotic oxamyl degradation in the presence of Fe^{II}. Adapted from Bromilow et al. (1986) and Strathmann and Stone (2001).

(DMTO), methylamine, and CO_2. Rates of oxamyl elimination are proportional to $[OH^-]$ and independent of Fe^{II} concentration or speciation (Strathmann and Stone, 2002a). A net two-electron reduction of oxamyl, occurring in parallel with the elimination reaction, can be coupled with the one-electron oxidation of two Fe^{II} ions. The products of oxamyl reduction include a nitrile (DMCF), methanethiol, methylamine, and CO_2. Details of the corresponding reduction and elimination pathways for methomyl and aldicarb are provided elsewhere (Bank and Tyrell, 1984; Bromilow et al., 1986; Strathmann and Stone, 2001).

Dissolved inorganic and organic ligands dramatically affect the kinetics of OCP reduction, but have no effect on OCP elimination (Strathmann and Stone, 2002a, 2002b). Reduction rates varied by nearly 6 orders of magnitude under conditions examined, and kinetics were found to be related to Fe^{II} speciation by the following expression:

$$k_{red} = [Fe^{II}]\sum_i k_i \alpha_i \qquad (1)$$

where k_{red} (h^{-1}) is the pseudo first-order rate constant for OCP reduction by an excess concentration of Fe^{II}, $[Fe^{II}]$ is the total dissolved Fe^{II} concentration, and k_i and α_i are the bimolecular rate constant $(m^{-1}\ h^{-1})$ and fractional concentration of each Fe^{II} species, respectively (Strathmann and Stone, 2002a, 2002b). In general, Fe^{II} complexation by Fe^{III}-stabilizing ligands leads to significant increases in the rates of OCP reduction. A linear free energy relationship (LFER) is observed between $\log k_i$ and standard one-electron reduction potentials of corresponding Fe^{III}/Fe^{II} redox couples ($E_H°$, in volts) (Strathmann and Stone, 2002b). Fe^{II} species in which five or six coordination positions are occupied by the complexing ligand (e.g., $Fe^{II}EDTA^{2-}$) are an exception to this relationship; $\log k_i$ values are significantly lower than those predicted by the LFER, which can be interpreted as interference with an inner-sphere OCP reduction pathway (Strathmann and Stone, 2002b). OCPs are predicted to be present as neutral nonionic species throughout the pH range studied (Strathmann and Stone, 2002a), and no effect of OCP speciation was observed.

We expect that mineral surfaces present in soil and aquifer material affect OCP reduction kinetics by influencing Fe^{II} speciation in a similar manner as solution-phase ligands. Rapid reduction of OCPs has been observed in $Fe(OH)_2(s)$ suspensions (Strathmann and Stone, 2002a) and in suboxic soil suspensions containing Fe^{II} (Bromilow et al., 1986; Dean et al., 2000; Warren et al., 2000). However, the speciation of Fe^{II} in these systems is unclear, rendering it difficult to determine which constituents and/or Fe^{II} species are responsible for OCP reduction.

This study examines the reduction of OCPs in suspensions containing Fe^{II} and well-defined mineral phases. Minerals selected for this study represent a range of surfaces encountered in soils and groundwater. Many of them have been utilized in previous low-temperature geochemical studies. Properties of the mineral phases vary considerably (e.g., bulk crystal structure, surface metal identity, specific surface area, acid-base characteristics). By measuring kinetics as a function of surface identity, surface area loading, pH, and extent of Fe^{II} adsorption, we are able to assess the influence of these factors on OCP

reduction. As with our previous work, emphasis is placed on correlating observed reaction rates with Fe^{II} speciation. By doing so, we are able to compare the reactivity of Fe^{II} adsorbed on different surfaces with the reactivity of solution-phase Fe^{II} species.

2. MATERIALS AND METHODS

2.1. Experimental Setup

Because strict oxygen exclusion was required, all experiments were carried out inside a controlled-atmosphere glove box (95% N$_2$, 5% H$_2$; Pd catalyst; Coy Laboratory Products, Grass Lake, MI) using distilled, deionized water (DDW) with resistivity of 18 MΩ-cm (Millipore Corp., Milford, MA). Before use, DDW was autoclaved and then sparged (>3 h/L) with ultra-high purity nitrogen (5.0 grade; BOC gases, Baltimore, MD) before and immediately after being placed in the glovebox. Stock mineral suspensions were de-oxygenated by thorough sparging with ultra-high purity nitrogen. All salt and buffer solutions were prepared in deoxygenated DDW and were filtered (0.22-μm Millipore Millex-GS) before use. Stock solutions of Fe^{II} were prepared and calibrated as previously described (Strathmann and Stone, 2001). All glassware/plasticware was soaked in concentrated HNO$_3$ and rinsed several times with DDW before use. Glassware/plasticware having prior contact with iron-containing solutions was also soaked in a mixture of ascorbic acid and oxalic acid before soaking in HNO$_3$.

2.2. Chemical Reagents

All chemicals were of the highest purity available. Oxamyl, methomyl, oxamyl oxime, methomyl oxime, and N,N-dimethyl-1-cyanoformamide (DMCF) were provided by DuPont Crop Protection (Wilmington, DE). Aldicarb was provided by Rhône-Poulenc Agriculture Limited (Essex, England). FeCl$_2 \cdot$ 4H$_2$O, FeCl$_3 \cdot$ 6H$_2$O, NaCl, NaClO$_4$, NaOH, sodium acetate (buffer; pK_a = 4.75), 2-(N-morpholino)ethanesulfonic acid monohydrate (MES buffer; pK_a = 6.1) and 3-(2-Pyridyl)-5,6-bis(4-phenylsulfonic acid)-1,2,4-triazine monosodium salt monohydrate (Ferrozine colorimetric reagent) were purchased from Aldrich Chemical (Milwaukee, WI). Acetic acid and 3-(N-morpholino)propanesulfonic acid (MOPS buffer; pK_a = 7.2) were obtained from Sigma Chemical (St. Louis, MO). Acetonitrile, methanol, acetic acid, HNO$_3$, HClO$_4$ and HCl were purchased from J. T. Baker (Phillipsburg, NJ).

2.3. Mineral Phases

Nine synthetic and three naturally-occurring mineral phases were used in this study. These phases have previously been used in studies examining a wide range of mineral/water interfacial phenomena (e.g., Davies and Morgan, 1989; Nowack et al., 1996; Buerge and Hug, 1999). All synthetic minerals obtained from outside sources were reported to be high purity by the manufacturers. Aluminum oxide (γ-Al$_2$O$_3$; type Alumina-C), silicon dioxide #1 (amorphous fumed silica, type Aerosil OX50), silicon dioxide #2 (amorphous fumed silica, type Aerosil 200), and titanium dioxide #1 (type P-25) were provided by Degussa (Frankfurt, Germany). Titanium dioxide #2 was obtained from TiOxide (Cleveland, England). Titanium dioxide #3 was obtained from Alfa Aesar (Ward Hill, MA). Kaolinite #1 (KGa-2) and kaolinite #2 (KGa-1B), both originating from natural deposits in Georgia, were purchased from the Clay Mineral Society's Source Clay Repository (Columbia, MO). Silicon dioxide #3 (ground quartz, Min-U-Sil 5) was obtained from U.S. Silica (Berkeley Springs, WV). Aluminum oxides, silicon dioxides, titanium dioxides, and kaolinites were used as received; they were stored in powder form at 110°C before preparation of aqueous suspensions. Hematite #1 was prepared for this study according to a procedure outlined in Penn et al. (2001). Hematite #2 and goethite were prepared by the procedures described by Vasudevan and Stone (1998). The iron (hydr)oxides were then stored in aqueous suspension before use. Suspensions of hematite #2 and goethite were aged for ~5 yr at 4°C in darkness before their use in this study. To ensure complete hydration of mineral surfaces, aqueous stock suspensions of all other mineral phases were prepared at least 1 d before their use in kinetic and adsorption experiments.

2.4. Mineral Characterization

The bulk crystal structures of the mineral phases were assessed by powder X-ray diffraction (XRD). XRD analysis was performed on a Philips diffractometer (XRG 3100 X-ray generator) utilizing CuKα radiation. Minerals were identified by comparing diffraction patterns with a library of standard mineral phases (Jade XRD, Livermore, CA).

The particle size and morphology of selected mineral phases were assessed using transmission electron microscopy (TEM). TEM analysis was carried out using Philips 420T and Philips CM300FEG transmission electron microscopes. TEM analysis of most minerals used here were reported in a prior study (Vasudevan and Stone, 1998). TEM analysis of goethite and hematite #1 were carried out in this study. Images of hematite #1 and goethite are provided elsewhere (Penn et al., 2001; Strathmann, 2001).

The specific surface area (m^2 g^{-1}) of each mineral was determined by five-point B.E.T. analysis (Fridrikhsberg, 1986) of N$_2$ adsorption on powdered samples at 77 K (SA 3100 analyzer; Beckman-Coulter, Miami, FL). Powdered iron oxide samples were obtained by freeze-drying aqueous suspensions.

2.5. Kinetic Experiments

OCP degradation experiments were performed in 250-mL polypropylene containers. Reaction suspensions were prepared by mixing together appropriate pH buffer, NaCl, particulate mineral phase, and FeCl$_2$ from de-oxygenated aqueous stock solutions. After equilibrating the resulting suspensions overnight, a small volume of OCP was added from a de-oxygenated aqueous stock solution to initiate each reaction. The initial OCP concentration was 25 μmol/L, and the initial total Fe^{II} concentration was 0.5 mmol/L in all reactions. Ionic strength was ~100 mmol/L for most reactions; only small differences in kinetics were observed at lower ionic strength (5 mmol/L). All reactions were carried out at pH < 7.5 to maintain undersaturation with respect to the thermodynamic solubility product for Fe(OH)$_2$(s) reported by Feitknecht and Schindler (1963). Although surface-induced precipitation of Fe(OH)$_2$(s) or similar phases cannot be ruled out, the likelihood of surface-induced precipitation was minimized by utilizing short preequilibration times (~12 h) and maintaining Fe^{II} surface coverages (ratio of adsorbed Fe^{II} concentration to estimated concentration of surface sites) well under monolayer coverage.

Sealed reactors were continuously mixed under darkness in a constant temperature circulating water bath (25.0 ± 0.1°C) within the glovebox. Special care was taken to ensure that mineral particles were uniformly suspended in solution during each reaction. Reactions were typically monitored for three half-lives. At least five, but in most cases several more, aliquots of suspension were collected for analysis at approximately equal time intervals. To quench the reactions, aliquots of suspension were filtered to remove mineral particles and adsorbed Fe^{II} (0.22-μm Millipore Millex-GS), passed through a cation exchange resin to remove dissolved Fe^{II} (OnGuard-H; Dionex, Sunnyvale, CA), and acidified with HCl to inhibit the OH$^-$-catalyzed E1cb elimination reaction (Fig. 2). The aqueous-phase concentration of the OCPs and their transformation products were then determined by HPLC analysis using methods described previously (Strathmann and Stone, 2001, 2002b). The suspension pH was measured periodically during the course of each reaction (Fisher Accumet 825MP meter with Orion combination semimicro probe; NIST standard buffers); these measurements demonstrated that pH was stable to within 0.05 units.

Fe^{II}-free control experiments were conducted for each mineral phase to account for any non-reductive loss processes (e.g., OCP adsorption, mineral-catalyzed elimination). In a prior study, rates of OCP degradation in homogeneous solution were measured using the same experimental setup (Strathmann and Stone, 2002a); these reactions served as mineral-free controls.

2.6. Fe^{II} and OCP Adsorption

The extent of Fe^{II} adsorption onto mineral surfaces was measured in batch reactors of the same solution composition used in kinetic exper-

iments (without OCPs present). Samples were allowed to equilibrate overnight, the same amount of time that kinetic batch reactors were allowed to equilibrate before adding the OCPs. Aliquots of each suspension were then collected by syringe and passed through a series of two filters (0.22-μm Millipore Millex-GS filter + 0.02-μm Anatop 25-Plus inorganic membrane filter; Whatman Scientific, Maidstone, England). An excess of buffered (pH 7.0) ferrozine colorimetric reagent was then added to the filtrate, and dissolved Fe^{II} concentration was determined spectrophotometrically at 562 nm (UV-160; Shimadzu, Kyoto, Japan) (Stookey, 1970). Adsorbed Fe^{II} concentration was then calculated by difference.

With the exception of the aluminum oxide suspensions, adsorbed Fe^{II} could be completely recovered from mineral surfaces by acidifying suspensions to pH 1 with HCl. This confirmed that the decrease in dissolved Fe^{II} measured in above experiments is due solely to reversible adsorption processes, and that non-reversible Fe^{II} adsorption and/or Fe^{II} oxidation by solution constituents (other than OCPs) is negligible.

In repeated experiments, a significant fraction of measured Fe^{II} adsorption onto aluminum oxide surfaces (~20% of total Fe^{II}) could not be recovered by either acidification or addition of the chelating agent EDTA. Extreme care was taken to ensure O_2 exclusion from our experimental setup, so we do not believe that Fe^{II} oxidation by O_2 contamination is responsible for incomplete recovery of Fe^{II} in aluminum oxide suspensions. Incomplete recovery of adsorbed metal ions is commonly attributed to rapid adsorption onto exterior oxide surfaces followed by slow diffusion of metal ions into internal binding sites and fixation at positions within the oxide particles (Bruemmer et al., 1988; Coughlin and Stone, 1995). Others have attributed incomplete recovery of adsorbed metal ions to the formation of new insoluble phases that incorporate the adsorbing metal ion (Jeon et al., 2001).

Experiments were also carried out to assess the extent of OCP adsorption onto mineral surfaces. Twenty-five μmol/L of each OCP was added to 5 g L^{-1} Fe^{II}-free suspensions of each mineral (25°C, pH 5.5, 25 mmol/L MES, 100 mmol/L NaCl). After equilibrating for 1 h, samples were collected by syringe and filtered in the same manner as in Fe^{II} adsorption experiments. The filtrate was then examined by HPLC, and the extent of OCP adsorption was calculated by comparing filtrate concentrations with a mineral-free control. These experiments indicate minimal adsorption of OCPs (<5% of total) under the conditions examined here.

2.7. Kinetic Data Analysis

Kinetic data were analyzed using the software package Scientist for Windows (v. 2.01, Micromath, Salt Lake City, UT). Pseudo first-order rate constants for OCP breakdown via reduction (k_{red}, h^{-1}) and the parallel OH^--catalyzed elimination reaction (k_{elim}, h^{-1}) were determined for individual batch reactions as described previously (Strathmann and Stone, 2001). Numerically integrated solutions to a system of differential rate expressions:

$$-\frac{d[OCP]}{dt} = (k_{red} + k_{elim})[OCP] \qquad (2)$$

$$\frac{d[\text{Nitrile Reduction Product}]}{dt} = k_{red}[OCP] \qquad (3)$$

$$\frac{d[\text{Oxime Elimination Product}]}{dt} = k_{elim}[OCP] \qquad (4)$$

were fit (method of least squares) to experimental data for both parent OCP loss and reaction product appearance. By fitting product formation data simultaneously with parent compound loss data, we are better able to assess the importance of each reaction pathway to overall OCP degradation. For most reactions monitored in this study, $k_{elim} \ll k_{red}$, hence the elimination pathway can be ignored when analyzing kinetics. For aldicarb, degradation products were not identified; values of k_{red} were calculated as the difference between pseudo first-order rate constants for aldicarb loss ($k_{obs} = k_{red} + k_{elim}$) measured in the presence and absence of Fe^{II}, respectively. Only pseudo first-order rate constants > 7.0 × 10^{-5} h^{-1} can be reliably calculated using our experimental approach and data analysis methods.

Table 1. Characteristics of mineral particles.

Mineral	Structural formula[a]	BET surface area (m^2 g^{-1})	pH$_{ZPC}$
Hematite #1	α-Fe$_2$O$_3$	64.5	8.5[e]
Hematite #2	α-Fe$_2$O$_3$	80.1	8.5[e]
Goethite	α-FeOOH	48.0	8.5[e]
Titanium dioxide #1	TiO$_2$ (anatase/rutile)	39.5[d]	6.3[f]
Titanium dioxide #2	TiO$_2$ (rutile)	3.5[d]	6.1[g]
Titanium dioxide #3	TiO$_2$ (anatase)	8.9[d]	6.3[f]
Kaolinite #1	Al$_2$Si$_2$O$_5$(OH)$_4$[b]	19.9	4.9[b]
Kaolinite #2	Al$_2$Si$_2$O$_5$(OH)$_4$[b]	11.3	5.1[b]
Aluminum oxide	γ-Al$_2$O$_3$[c]	90.1[d]	7.8[h]
Silicon dioxide #1	SiO$_2$ (amorphous)	47.6	2.4[i]
Silicon dioxide #2	SiO$_2$ (amorphous)	208	2.4[i]
Silicon dioxide #3	SiO$_2$ (ground quartz)	4.9	2.4[i]

[a] Determined by powder x-ray diffraction.
[b] Sutheimer et al. (1999).
[c] Kummert and Stumm (1980).
[d] Vasudevan and Stone (1998).
[e] Liger et al. (1999).
[f] Torrents (1992).
[g] Hayes et al. (1991).
[h] Nowack et al. (1996).
[i] Young (1982).

Scientist was also used to calculate the bimolecular rate constants (m^{-1} h^{-1}) for oxamyl reduction by Fe^{II} adsorbed onto different mineral surfaces. Experimental kinetic and adsorption data were fit (method of least squares) by an expanded form of Eqn. 1 that includes both dissolved and adsorbed Fe^{II} species (Eqn. 8, discussed below). For model fitting purposes, rate constants for oxamyl reduction by dissolved Fe^{II} species (e.g., Fe^{2+}, $Fe[OH]_2^0$) were fixed at the values determined from a previous analysis of Fe^{II} reactivity in mineral-free solutions (Strathmann and Stone, 2002a).

3. RESULTS AND DISCUSSION

3.1. Mineral Characterization

Selected properties of the mineral phases examined in this study are listed in Table 1. The mineral phases are built from four different metal ions that are abundant in soil: Fe^{III}, Ti^{IV}, Al^{III}, and Si^{IV}. The particles exhibit a wide range of crystal structures, B.E.T. surface areas (3.5–208 m^2 g^{-1}) and surface acidities as measured by the pH of zero proton charge (pH$_{ZPC}$: 2.4–8.5) (Kummert and Stumm, 1980; Young, 1982; Liang, 1988; Davies and Morgan, 1989; Hayes et al., 1991; Torrents, 1992; Vasudevan and Stone, 1998; Sutheimer et al., 1999). Nine of the mineral phases are synthetic and three originate from natural formations (kaolinites #1 and #2, and SiO$_2$ #3).

The minerals also exhibit a wide range in particle morphology and size. TEM analysis indicates that hematites #1 and #2 are indistinguishable; both are well-defined crystalline phases and consist of isometric particles of size 20 to 25 nm that form by oriented aggregation of smaller primary particles (Penn et al., 2001). Goethite is a well-defined crystalline phase and consists of prismatic acicular crystals that form parallel aggregates of length 500 nm and width 100 nm. Titanium dioxides #1 and #3 are well-defined crystalline phases and consist of isometric/octahedral particles with diameters of 30 and 200 nm, respectively (Vasudevan and Stone, 1998). Titanium dioxide #2 consists of elongated and irregular-shaped prismatic particles that form radial aggregates ~1 μm in size (Vasudevan and

Stone, 1998). Aluminum oxide is a predominantly crystalline phase and consists of isometric/hexagonal particles of diameter 20 nm (Vasudevan and Stone, 1998). Kaolinite #1 is a poorly-defined crystalline phase and consists of rounded hexagonal particles of diameter 450 nm and thickness 40 nm (Sutheimer et al., 1999). Kaolinite #2 is a well-defined crystalline phase and consists of hexagonal particles of diameter 800 nm and thickness 60 nm (Sutheimer et al., 1999). Silicon dioxides #1 and #2 are X-ray amorphous phases and are reported by the manufacturer to consist of non-porous spherical particles of diameter 40 and 12 nm, respectively. Silicon dioxide #3 is described by the supplier as consisting of fine-ground quartz (confirmed by XRD) particles with mean diameter 1.6 μm.

3.2. E1 cb Elimination Kinetics

In Fe[II]-free mineral suspensions, no OCP reduction is observed. Instead, OCPs degrade solely via the established base-catalyzed elimination pathway (E1cb mechanism) illustrated in Figure 2 for oxamyl (Hegarty and Frost, 1973; Huang, 1997; Strathmann and Stone, 2001). Rates of OCP elimination measured in suspensions of each mineral phase are not significantly different from rates measured in mineral-free solution at the same pH (rates agree within a factor of 1.3) (Strathmann and Stone, 2002a). Similarly, the presence of Fe[II] does not significantly affect k_{elim} measurements in either the absence or presence of mineral phases. As a result, we conclude that the mineral surfaces examined in this study do not significantly catalyze or inhibit the E1cb elimination reactions of OCPs. This contrasts with the findings of Zhang and co-workers (personal communication), who observed significant catalysis of the oxamyl elimination in suspensions of iron-bearing smectite clays. These investigators believe that the mechanism for catalysis involves oxamyl reacting at interlayer regions within the smectite structure; minerals examined in the present study do not contain similar interlayer regions.

3.3. Oxamyl Reduction Kinetics

In solutions containing both Fe[II] and mineral surfaces, rates of oxamyl degradation are significantly faster than in the absence of either component. Reaction time courses observed in mineral suspensions are similar to those reported for homogeneous solution containing Fe[II] (Bromilow et al., 1986; Strathmann and Stone, 2001). Oxamyl degradation follows pseudo first-order kinetics, and results in the formation of both DMCF (nitrile reduction product) and oxamyl oxime (E1 cb elimination product). These two products provide a good mass balance (near 100% in all reactions monitored) for the amount of oxamyl degraded. The good mass balance also demonstrates that neither oxamyl nor its degradation products adsorb significantly to the mineral surfaces.

As an illustrative example, Figure 3 shows a time course for oxamyl degradation in a suspension containing Fe[II] and goethite. The model fits of both oxamyl loss and reaction product formation demonstrate good agreement with the pseudo first-order kinetic model that considers parallel reduction and elimination reactions (Eqn. 2–4), as was reported in our earlier studies on oxamyl degradation in homogenous solutions (Strathmann and Stone, 2001, 2002a, 2002b). For the model fits
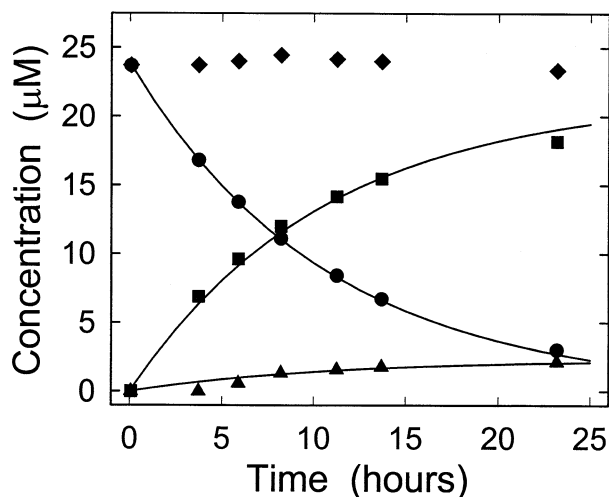

Fig. 3. Time course for oxamyl degradation in the presence of 0.5 mmol/L Fe[II] and 48 m^2 L^{-1} goethite at pH 7.4 (25 mmol/L MOPS buffer), 100 mmol/L NaCl, and 25°C. Symbols represent measured concentrations of oxamyl (●), DMCF (■), oxamyl oxime (▲), and mass balance (◆). Lines represent pseudo first-order model fit, using $k_{red} = 8.45 \ (\pm 0.38) \times 10^{-2} \ \text{h}^{-1}$ and $k_{elim} = 9.18 \ (\pm 1.83) \times 10^{-3} \ \text{h}^{-1}$.

shown, $k_{red} = 8.45 \ (\pm 0.38) \times 10^{-2} \ \text{h}^{-1}$ and $k_{elim} = 9.18 \ (\pm 1.83) \times 10^{-3} \ \text{h}^{-1}$. This compares with $k_{red} = 9.08 \ (\pm 0.17) \times 10^{-3} \ \text{h}^{-1}$ and $k_{elim} = 8.72 \ (\pm 0.17) \times 10^{-3} \ \text{h}^{-1}$ determined at the same pH in homogeneous solution containing the equivalent concentration of Fe[II] (uncertainty represents 95% confidence limits). Hence, the addition of goethite significantly catalyzes reduction, but not elimination. In fact, for most of the mineral phases examined, OCP reduction is so fast that elimination products are not detected at all.

Several studies have pointed out that reactions involving Fe[II] are markedly affected by changing the mineral surface area loading (S_{AL}; m^2 surface area per liter of solution) or suspension pH (Tamura et al., 1980; Klausen et al., 1995; Buerge and Hug, 1999; Liger et al., 1999; Amonette et al., 2000; Schultz and Gundl, 2000; Vikesland and Valentine, 2002). Figure 4 illustrates that oxamyl reduction is also considerably affected by these same factors. Figure 4A shows that rates of oxamyl disappearance in suspensions of hematite #1 increase significantly when the S_{AL} increases while holding pH and total Fe[II] concentration constant. Likewise, Figure 4B shows that rates of oxamyl disappearance increase when suspension pH increases while holding S_{AL} and total Fe[II] concentration constant. Again, model fits indicate pseudo first-order kinetics is followed, and with the exception of the hematite-free control, > 90% of parent compound loss shown in the time courses is accounted for by the formation of reduction product (i.e., $k_{red} \gg k_{elim}$).

It is expected that the enhanced rates of oxamyl reduction observed in mineral suspensions result from Fe[II] adsorption onto particle surfaces. The effects that hematite S_{AL} and pH have on the kinetics of oxamyl reduction follow the same pattern generally reported for Fe[II] adsorption onto metal (hydr) oxide and aluminosilicate surfaces. That is, the extent of Fe[II] adsorption (moles of Fe[II] adsorbed per liter of suspension) onto a given mineral surface increases with S_{AL} and pH (Coughlin and Stone, 1995; Klausen et al., 1995; Buerge and Hug, 1999;

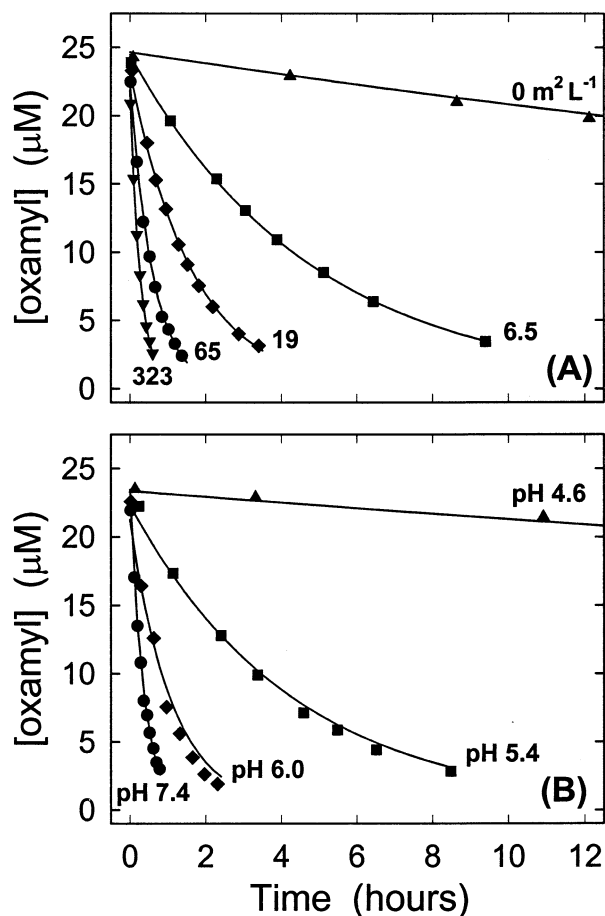Fig. 4. Oxamyl reduction by 0.5 mmol/L Fe^{II} in the presence of hematite #1 (α-Fe_2O_3): (A) Effect of varying surface area loading (S_{AL}, $m^2\,L^{-1}$) at pH 7.4, (B) effect of varying pH in the presence of 129 $m^2\,L^{-1}$ hematite. Symbols indicate measured concentrations and lines indicate pseudo first-order model fits. Reaction conditions: 0.5 mmol/L total Fe^{II}, 25 μmol/L oxamyl, 25°C, 100 mmol/L NaCl, pH 4.6 to 7.4 (5 mmol/L acetate, 25 mmol/L MES, 25 mmol/L MOPS buffers), S_{AL} = 0 to 323 $m^2\,L^{-1}$.

Liger et al., 1999; Vikesland and Valentine, 2002), typical of transition metal ions. Hydrated metal (hydr)oxide surfaces are covered with various oxygen donor ligands (e.g., ≡S-OH) that can bind metal ions in the same manner as dissolved oxygen donor ligands (e.g., OH^-, HCO_3^-, oxalate) (Stumm, 1992). Increasing S_{AL} affects Fe^{II} adsorption by increasing the total concentration of surface-bound oxygen donor ligands (moles per liter of suspension). Meanwhile, the effect of changing pH on Fe^{II} adsorption can be traced to the competition between Fe^{II} and H^+ (or other metal ions) for the surface-bound oxygen donor ligands (Stumm, 1992). As $[H^+]$ decreases with increasing pH, the competition for surface-bound ligands shifts more in favor of Fe^{II}.

By analogy with solution-phase Fe^{II} complexes, we expect mineral surfaces to catalyze oxamyl reduction if surface-complexed Fe^{II} species are kinetically more reactive than Fe^{2+}_{aq}. Conversely, mineral surfaces will inhibit oxamyl reduction if surface-complexed Fe^{II} species are kinetically less reactive than Fe^{2+}_{aq}. The kinetic reactivity of surface-complexed Fe^{II} has often been attributed to the effect that surface complexation

has on the thermodynamics of the Fe^{III}/Fe^{II} redox couple (Wehrli et al., 1989; Buerge and Hug, 1999). This interpretation follows from the observed relationship between the kinetic reactivity of solution-phase Fe^{II}-ligand complexes and the one-electron reduction potential (E_H°) of the corresponding Fe^{III}-ligand/Fe^{II}-ligand redox couples (Buerge and Hug, 1998; King and Farlow, 2000; Strathmann and Stone, 2002a, 2002b). That said, mineral surface catalysis of oxamyl reduction is likely to involve other mechanisms in addition to the effect on E_H° (see section 3.9).

3.4. Effect of Mineral Surface Area

A series of experiments were carried out to quantify Fe^{II} adsorption and k_{red} for oxamyl as a function of S_{AL} at pH 7.4 in suspensions of each mineral. Results of these experiments are illustrated in Figures 5 and 6. The upper portion of each panel shows the extent of Fe^{II} adsorption, and the lower portion indicates the corresponding kinetic measurements. Initial total Fe^{II} and oxamyl concentrations in kinetic experiments were 0.5 mmol/L and 25 μmol/L, respectively. Solution conditions were identical for Fe^{II} adsorption experiments, with the exception that oxamyl was excluded. The range in S_{AL} examined for each mineral varied because of difficulty filtering high S_{AL} suspensions of particular minerals (e.g., SiO_2 #3). For most minerals, however, we examined mass loadings from 0 to 10 g L^{-1}.

For each mineral surface, Fe^{II} adsorption increases linearly with increasing S_{AL} until $[Fe^{II}]_{ads}$ approaches $[Fe^{II}]_{total}$, at which point it plateaus off with further increases in S_{AL} (note the axis; these are not plotted in the same manner as Langmuir adsorption isotherms). The maximum extent of Fe^{II} adsorption varies considerably from one mineral surface to another. For some surfaces, the extent of Fe^{II} adsorption reaches nearly 100% of added Fe^{II} under conditions examined (both hematites, goethite, TiO_2 #1, #3, and γ-Al_2O_3). For other surfaces, very little Fe^{II} adsorption is observed even at the highest S_{AL} examined (TiO_2 #2, SiO_2 #1–#3, and kaolinite #1, #2). In fact, because Fe^{II} adsorption onto the SiO_2 surfaces is extremely weak and proved difficult to measure reproducibly at the S_{AL} conditions used in kinetic experiments, we chose to estimate adsorption under these conditions by linear extrapolation from the amount of Fe^{II} adsorbed in 50 g L^{-1} suspensions (estimates indicated by dashed lines Figs. 6D–6F). A similar procedure was used by Buerge and Hug (1999) to estimate Fe^{II} adsorption onto SiO_2 #1 at conditions used in Cr^{VI} reduction experiments.

Kinetic measurements of oxamyl reduction in the mineral suspensions (Figs. 5 and 6, lower portions of each panel) follow the same general pattern as the extent of Fe^{II} adsorption. For each mineral, k_{red} increases with increasing S_{AL}, and for some surfaces, k_{red} approaches a maximum at S_{AL} values corresponding to those where the extent of Fe^{II} adsorption approaches $[Fe^{II}]_{tot}$. The parallel trends support our hypothesis that surface catalysis occurs as a result of Fe^{II} complexation by surface-bound ligand donor groups.

The overall degree of surface catalysis varies considerably from one surface to another. For example, even though the extent of Fe^{II} adsorption increases from 0 to nearly 100% of $[Fe^{II}]_{tot}$ for all three iron (hydr)oxides, k_{red} increases only 12-fold for goethite vs. 500-fold for the two hematite minerals. Therefore, the reactivity of an equivalent concentration of
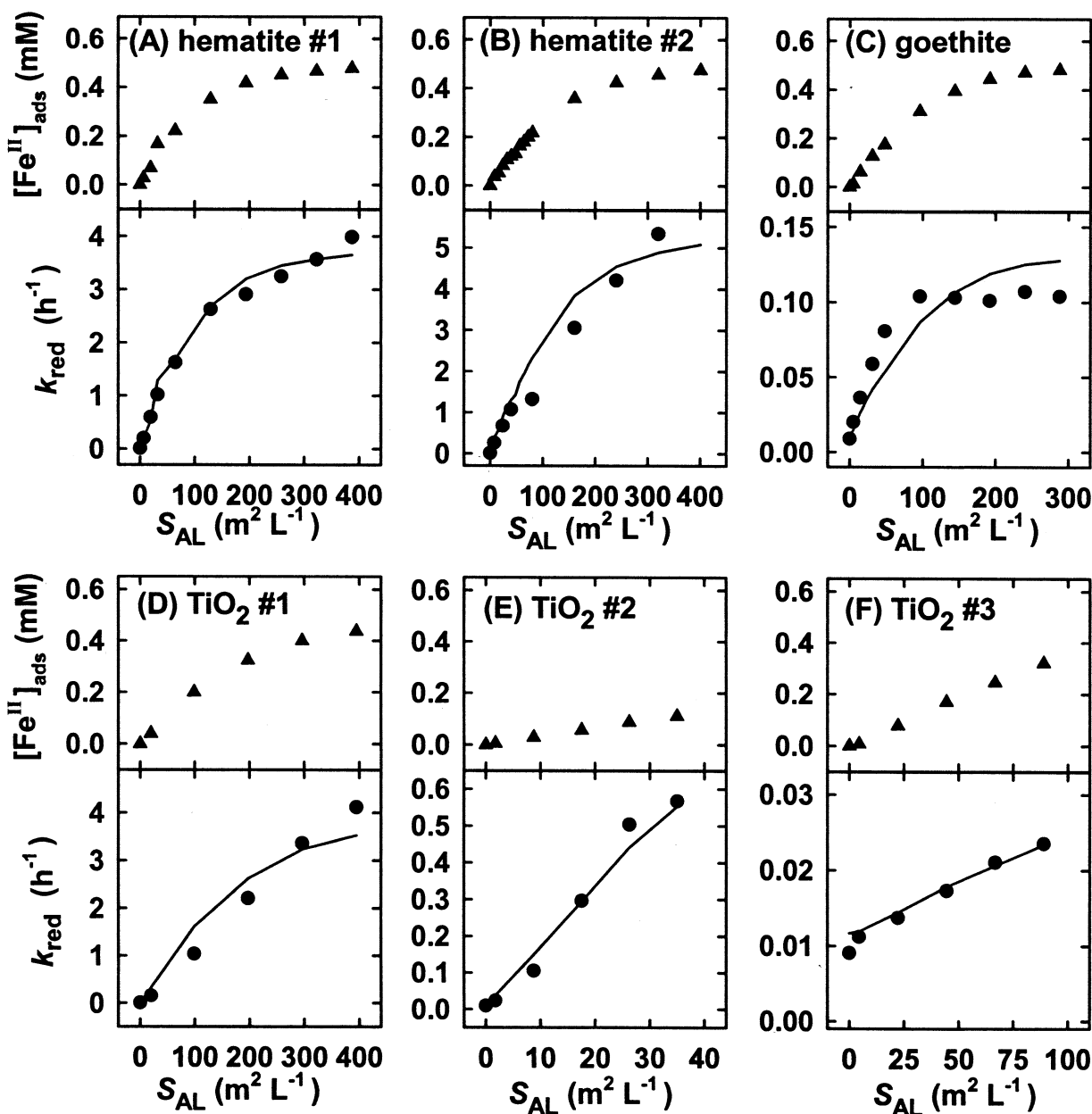
Fig. 5. Extent of Fe^{II} adsorption and pseudo first-order rate constant for oxamyl reduction, k_{red}, as a function of S_{AL} in suspensions of various iron (hydr)oxide and titanium dioxide minerals. Symbols represent measured Fe^{II} adsorption (▲) and measured k_{red} (●). Lines in lower panels indicate predicted values of k_{red} using Eqn. 8 and the rate constants reported in Table 2. Reaction conditions: pH 7.4 (25 mmol/L MOPS), 0.5 mmol/L total Fe^{II}, 25 μmol/L oxamyl, 25°C, 100 mmol/L NaCl, 25 mmol/L MOPS.

adsorbed Fe^{II} with oxamyl varies with the identity of the adsorbing mineral surface. This is not surprising given the wide variation in reactivity observed for different solution-phase Fe^{II} complexes (Strathmann and Stone, 2002a, 2002b).

3.5. Effect of pH

The effect of changing pH on Fe^{II} adsorption and k_{red} for oxamyl was also examined for four mineral surfaces. The initial Fe^{II} and oxamyl concentrations were the same as above. Re-

sults of these experiments are shown in Figure 7. As expected, the degree of Fe^{II} adsorption is lowest under acidic conditions, and increases significantly over a narrow pH range just below neutral pH; the degree of adsorption goes from negligible to nearly 100% in just 2 pH units. Similar Fe^{II} adsorption behavior has been reported previously for both metal (hydr)oxides and aluminosilicates (Coughlin and Stone, 1995; Klausen et al., 1995; Liger et al., 1999; Jeon et al., 2001; Vikesland and Valentine, 2002).
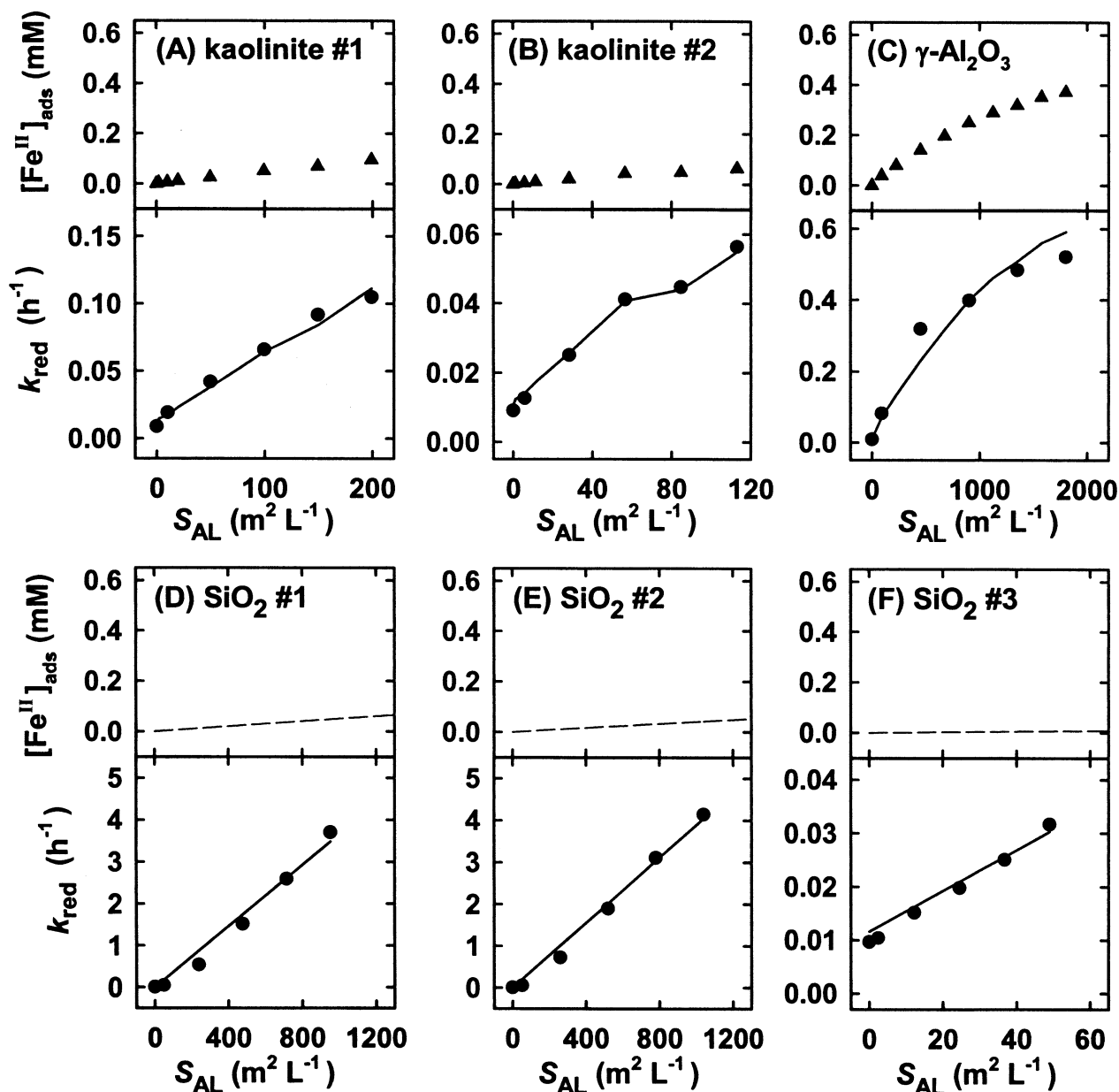
Fig. 6. Extent of Fe^{II} adsorption and pseudo first-order rate constant for oxamyl reduction, k_{red}, as a function of the S_{AL} in suspensions of various kaolinite, aluminum oxide and silicon dioxide minerals. Symbols represent measured Fe^{II} adsorption (▲) and measured k_{red} (●). Fe^{II} adsorption onto SiO_2 surfaces calculated by linear extrapolation from measurements in 50 g L^{-1} suspensions (indicated by dashed lines in upper panels). Lines in lower panels indicate predicted values of k_{red} using Eqn. 8 and the rate constants reported in Table 2. Reaction conditions: pH 7.4 (25 mmol/L MOPS), 0.5 mmol/L total Fe^{II}, 25 μmol/L oxamyl, 25°C, 100 mmol/L NaCl.

As with the variable-S_{AL} experiments described above, kinetic measurements of oxamyl reduction qualitatively follow the same general trend as the extent of Fe^{II} adsorption. Under acidic conditions, k_{red} measured in the presence of each mineral surface is indistinguishable from that measured in mineral-free solutions of the same composition ($\sim$4.5 $\times$ 10^{-3} h^{-1}). As pH increases, however, the rate of oxamyl reduction increases significantly. For example, in the presence of 129 m^2 L^{-1} of hematite #1, k_{red} for oxamyl at pH 7.4 is nearly 600-fold higher than the rate measured at pH 2.3. In comparison, k_{red} only

increases twofold for the same pH change in mineral-free solution. Again, the parallel between the trends in Fe^{II} adsorption and oxamyl reduction kinetics supports our hypothesis that surface catalysis occurs as a result of Fe^{II} complexation by surface-bound ligand donor groups.

3.6. Modeling Heterogeneous Oxamyl Reduction Kinetics

In mineral suspensions, we expect that oxamyl reduction proceeds along several parallel pathways, each reaction involv-
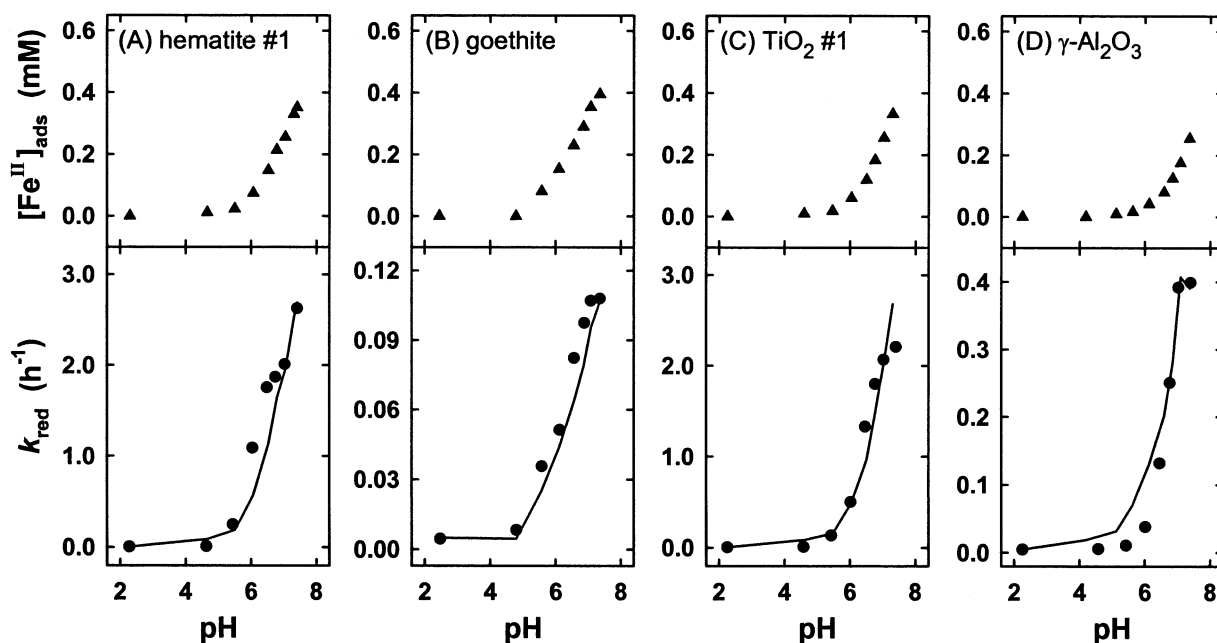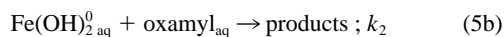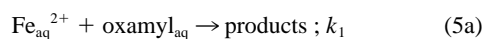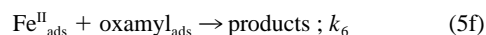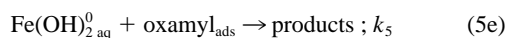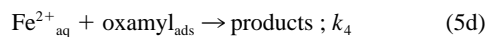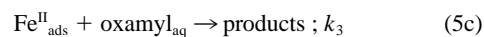
Fig. 7. Extent of Fe^II adsorption and k_{red} for oxamyl as a function of pH in selected mineral suspensions. Symbols represent measured Fe^II adsorption (▲) and measured k_{red} (●). Lines in lower panels indicate predicted values of k_{red} using Eqn. 8 and the rate constants reported in Table 2. Reaction conditions: pH 2 to 7.4 (10 mmol/L HCl, 5 mmol/L acetate, 25 mmol/L MES, 25 mmol/L MOPS), 0.5 mmol/L total Fe^II, 25 μmol/L oxamyl, 25°C, 100 mmol/L NaCl, 129 m^2 L^{-1} hematite #1, 144 m^2 L^{-1} goethite, 198 m^2 L^{-1} TiO$_2$ #1, and 901 m^2 L^{-1} γ-Al$_2$O$_3$

ing a different combination of reactants present either in the aqueous phase (aq) or adsorbed onto the mineral surface (ads). For example, we found in homogeneous solution (no added ligands present) that oxamyl$_{29}$ reduction kinetics can be adequately described by the reactions between oxamyl$_{aq}$ and two different Fe^II species, Fe$^{2+}_{aq}$ and Fe(OH)$_2^0{}_{aq}$ (Strathmann and Stone, 2002a):

$$Fe_{aq}^{2+} + oxamyl_{aq} \rightarrow products \; ; k_1 \qquad (5a)$$

$$Fe(OH)_{2\,aq}^0 + oxamyl_{aq} \rightarrow products \; ; k_2 \qquad (5b)$$

where k_1 and k_2 are the bimolecular rate constants (m^{-1} h^{-1}) for reduction of oxamyl$_{29}$ by Fe$^{2+}_{aq}$ and Fe(OH)$_2^0{}_{aq}$, respectively. Describing reaction kinetics in heterogeneous systems is inherently more complicated. Now, in addition to the two reactions listed above, we must also consider reactions that occur between two reactants present on the mineral surface (adsorbed species), as well as reactions where one reactant is adsorbed and one reactant is present in the overlying solution phase. Even if we assume only a single adsorbed Fe^II species and a single adsorbed oxamyl species, we now have to consider the following additional reactions:

$$Fe^{II}_{ads} + oxamyl_{aq} \rightarrow products \; ; k_3 \qquad (5c)$$

$$Fe^{2+}_{aq} + oxamyl_{ads} \rightarrow products \; ; k_4 \qquad (5d)$$

$$Fe(OH)_{2\,aq}^0 + oxamyl_{ads} \rightarrow products \; ; k_5 \qquad (5e)$$

$$Fe^{II}_{ads} + oxamyl_{ads} \rightarrow products \; ; k_6 \qquad (5f)$$

The following rate expression for oxamyl reduction can then be derived if we assume (1) that other pathways for oxamyl degradation are negligible compared to reduction, (2) that the adsorption/desorption and surface diffusion of reactants, intermediates, and products is rapid relative to electron transfer, and (3) that the kinetics of individual reactions listed in Eqn. 5a to 5f exhibit first-order dependence on the concentration of each reactant:

$$-\frac{d[oxamyl]}{dt} = k_1[Fe^{2+}]_{aq}[oxamyl]_{aq}$$

$$+ \; k_2[Fe(OH)_2^0]_{aq}[oxamyl]_{aq} + k_3[Fe^{II}]_{ads}[oxamyl]_{aq}$$

$$+ \; k_4[Fe^{2+}]_{aq}[oxamyl]_{ads} + k_5[Fe(OH)_2^0]_{aq}[oxamyl]_{ads}$$

$$+ \; k_6[Fe^{II}]_{ads}[oxamyl]_{ads} \qquad (6)$$

Eqn. 6 is similar to expressions derived for other surface catalyzed redox reactions (Deng and Stone, 1996; Buerge and Hug, 1999). This expression can be simplified further if we are able to assume that any of the individual reactions listed in Eqn. 5a to 5f are negligible. Experiments indicate that OCP adsorption onto mineral surfaces is minimal under conditions examined in this study (i.e., < 5% of total pesticide adsorbed). Hence, it may be feasible to neglect the contribution of reactions involving adsorbed oxamyl reacting with dissolved and adsorbed Fe^II (Eqn. 5d–5f). This simplifies Eqn. 6 to the following expression:

Table 2. Model-derived bimolecular rate constants for oxamyl reacting with Fe^{II} adsorbed onto selected mineral surfaces.[a,b]

Fe^{II} species	$k_3 \, m^{-1} \, h^{-1}$ $(m^{-1} \, h^{-1})$
$Fe^{2+}(aq)$	$9.27 \, (\pm 0.05)$[c]
$FeOH^+(aq)$	$< 2.5 \times 10^3$ [c]
$Fe(OH)_2^0(aq)$	$1.84 \, (\pm 0.11) \times 10^7$ [c]
$Fe^{II}(ads, hematite \#1)$	$7.64 \, (\pm 0.46) \times 10^3$
$Fe^{II}(ads, hematite \#2)$	$1.07 \, (\pm 0.16) \times 10^4$
$Fe^{II}(ads, goethite)$	$2.65 \, (\pm 0.26) \times 10^2$
$Fe^{II}(ads, TiO_2 \#1)$	$8.07 \, (\pm 0.82) \times 10^3$
$Fe^{II}(ads, TiO_2 \#2)$	$4.89 \, (\pm 1.14) \times 10^3$
$Fe^{II}(ads, TiO_2 \#3)$	$5.99 \, (\pm 0.73) \times 10^1$
$Fe^{II}(ads, kaolinite \#1)$	$1.07 \, (\pm 0.10) \times 10^3$
$Fe^{II}(ads, kaolinite \#2)$	$7.25 \, (\pm 0.86) \times 10^2$
$Fe^{II}(ads, \gamma\text{-}Al_2O_3)$	$1.58 \, (\pm 0.16) \times 10^3$
$Fe^{II}(ads, SiO_2 \#1)$	$7.27 \, (\pm 0.85) \times 10^4$
$Fe^{II}(ads, SiO_2 \#2)$	$9.76 \, (\pm 0.75) \times 10^4$
$Fe^{II}(ads, SiO_2 \#3)$	$3.07 \, (\pm 0.50) \times 10^3$

[a] Uncertainties for rate constants represent 95% confidence limits.
[b] Rate constants reported for mineral surfaces represents the mean sum reactivity of individual adsorbed Fe^{II} species.
[c] From Strathmann and Stone (2002a).

$$-\frac{d[oxamyl]}{dt} = k_1[Fe^{2+}]_{aq}[oxamyl]_{aq}$$

$$+ \, k_2[Fe(OH)_2^0]_{aq}[oxamyl]_{aq} + k_3[Fe^{II}]_{ads}[oxamyl]_{aq} \quad (7)$$

If total Fe^{II} is present in considerable excess of oxamyl, and if we assume that Fe^{II} equilibria are maintained, then it follows from Eqn. 1 that the pseudo first-order rate constant for oxamyl reduction can be described in terms of the fractional concentrations and bimolecular rate constants for dissolved oxamyl reacting with $Fe^{2+}{}_{aq}$, $Fe(OH)_2^0{}_{aq}$ and $Fe^{II}{}_{ads}$:

$$k_{red} = [Fe^{II}](k_1\alpha_{Fe(2+1)} + k_2\alpha_{Fe(OH)2} + k_3\alpha_{Fe(ads)}) \quad (8)$$

Least-squares model fits of Eqn. 8 to experimental data are shown in Figures 5 to 7. Model fits were carried out using k_3 as the only adjustable fitting parameter. k_{red} is measured, $\alpha_{Fe(ads)}$ is calculated from measured $[Fe^{II}]_{aq}$ by difference method, $\alpha_{Fe(2+)}$ and $\alpha_{Fe(OH)2}$ are calculated from measured $[Fe^{II}]_{aq}$ using appropriate stability constants (Martell et al., 1997), and k_1 and k_2 are fixed at the values measured in equivalent mineral-free solutions (Strathmann and Stone, 2002a). Values of k_3 obtained from model fits are listed in Table 2.

In general, Eqn. 8 adequately describes oxamyl reduction kinetics in mineral suspensions. Model fits agree closely with kinetic measurements in suspensions of each mineral phase. It is particularly noteworthy that a single value of k_3 is capable of accounting for kinetic trends observed when varying S_{AL} and when varying suspension pH. Figure 8 illustrates the close quantitative agreement between measured and model-predicted kinetics. Perfect agreement is represented by the 1-to-1 line. This plot clearly demonstrates that the majority of the model-predicted rate constants are in good agreement with experimental measurements. Model predictions are notably higher than measured values for a small number of points. However, most of these occur for low-pH samples where the extent of Fe^{II} adsorption is minimal and difficult to measure accurately using
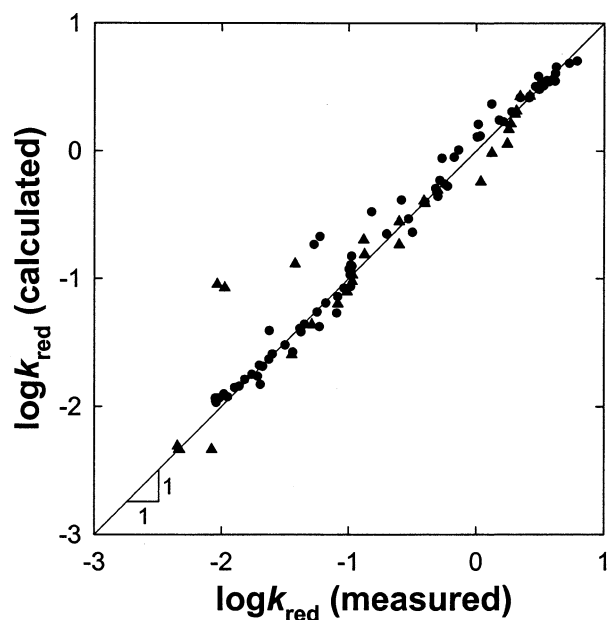

Fig. 8. Comparison of measured and model-predicted values of k_{red}. Data from varied-S_{AL} experiments (●) and data from varied-pH experiments (▲). Line indicates a perfect 1-to-1 match between experimental measurements and model predictions.

the difference method (see section 2.6); even small errors in $[Fe^{II}]_{ads}$ could cause these discrepancies at low pH.

The close agreement between the experimental results and model predictions suggests that the kinetics of oxamyl reduction is dependent upon total adsorbed Fe^{II}, rather than upon a particular subfraction of adsorbed Fe^{II}, which was reported for reactions with nitrobenzenes and U^{VI} (Charlet et al., 1998; Liger et al., 1999; Schultz and Gundl, 2000). That is, all the different Fe^{II} complexes that form on the surface of a given mineral phase can be kinetically described by a single species equal in concentration to the total adsorbed Fe^{II} (moles per liter of suspension), and reacting with oxamyl[29] according to the bimolecular rate constant k_3. Slight discrepancies between predicted and measured kinetics are observed in some suspensions, most notably in variable-S_{AL} experiments for goethite (Fig. 5C). This suggests that another kinetic model may be more appropriate in selected systems.

3.7. Assessment of Model Assumptions

The model used to describe oxamyl reduction in mineral suspensions assumes (1) that kinetics exhibit a first-order dependence on the concentration of each dissolved Fe^{II} species and a first-order dependence on the total concentration of Fe^{II} adsorbed onto the surface of a particular mineral (moles per liter of suspension), and (2) that the kinetic contribution of reactions involving adsorbed oxamyl is negligible and can be ignored (i.e., the last three terms in Eqn. 6 are much smaller than the first three terms). The model makes no assumptions regarding the structure of individual surface-complexed Fe^{II} species (i.e., mononuclear, binuclear, hydroxylated), the location on the surface where Fe^{II} adsorption occurs (i.e., terrace,

edge, kink sites), or Fe^{II} adsorption density (moles of adsorbed Fe^{II} per mole of surface adsorption sites).

Previous studies on the kinetic reactivity of Fe^{II} in mineral suspensions report conflicting kinetic dependencies with respect to adsorbed Fe^{II}. Buerge and Hug (1999) report that rates of Cr^{VI} reduction at pH 5.0 exhibit a first-order dependence on total adsorbed Fe^{II}, while Amonette et al. (2000) report that reduction of carbon tetrachloride exhibits a pH-independent second-order dependence on total Fe^{II} adsorbed. Other studies have reported a first-order dependence on the concentration of a subfraction of adsorbed Fe^{II}, rather than total adsorbed Fe^{II} (Charlet et al., 1998; Liger et al., 1999; Schultz and Gundl, 2000). For example, surface complexation modeling results reported by Charlet et al. (1998) indicate that Fe^{II} adsorption onto magnetite (Fe$_3$O$_4$) surfaces can be described by invoking two distinct stoichiometries, which they assign to mononuclear monodentate surface complexes of Fe^{2+} and FeOH$^+$ ($\equiv$S-OFe$^+$ and $\equiv$S-OFeOH^0, respectively). When these results were compared with kinetic trends for 4-chloronitrobenzene reduction in the same suspensions (Klausen et al., 1995), they found a correlation between initial rates of reduction and concentrations of $\equiv$S-OFeOH^0, rather than total adsorbed Fe^{II}. This suggests that, for some oxidants, different species of adsorbed Fe^{II} may exhibit markedly different reactivities.

According to Eqn. 7, kinetics should exhibit a first-order dependence on the concentration of each dissolved Fe^{II} species (i.e., Fe^{2+} and Fe(OH)$_2{}^0$ in our system) and a first-order dependence on total adsorbed Fe^{II} concentration. To assess the validity of the model, we need to first separate the kinetic contribution of reactions that occur at the surface of the mineral phases from those that occur in homogeneous aqueous solution. We can do this by dividing k_{red} into a solution-reaction contribution ($k_{red,sol}$, h^{-1}) and a surface-reaction contribution ($k_{red,surf}$, h^{-1}):

$$k_{red} = k_{red,sol} + k_{red,surf} \qquad (9)$$

Previous studies in this series (Strathmann and Stone, 2001, 2002a) demonstrated that the kinetics of solution-phase reaction exhibit first-order dependence on the concentrations of individual dissolved Fe^{II} species. Consequently, we are able to calculate $k_{red,sol}$ in mineral suspensions using measurements of dissolved Fe^{II} concentration, equilibrium constants for the formation of dissolved Fe(OH)$_2{}^0$, and values of k_1 and k_2 determined in homogeneous solutions:

$$k_{red,sol} = [Fe^{II}](k_1\alpha_{Fe(2+)} + k_2\alpha_{Fe(OH)2}) \qquad (10)$$

By difference we can then calculate $k_{red,surf}$ for each reaction. This term can then be used to determine the kinetic dependence of oxamyl reduction with respect to adsorbed Fe^{II} concentration and assess the model assumptions.

Figure 9 shows log-log plots for $k_{red,surf}$ (h^{-1}) for oxamyl in mineral suspensions, vs. total adsorbed Fe^{II} concentration. The slopes of the log-log plots indicate the kinetic dependence of the reaction on total adsorbed Fe^{II}. Slopes for the minerals examined range from 0.76 for goethite to 1.44 for SiO$_2$ #1. For most mineral surfaces, however, slopes are consistent with an assumed first-order dependence on total adsorbed Fe^{II} (i.e., a slope = 1.0 is within the 95% confidence limit). Data from both variable-S_{AL} and variable-pH experiments also fit onto the

same plots, suggesting that pH-dependent changes in the speciation of adsorbed Fe^{II} (as predicted by surface complexation modeling (Liger et al., 1999) do not significantly affect the observed reduction kinetics for oxamyl. For TiO$_2$ #1 and γ-Al$_2$O$_3$, there do appear to be some systematic trends in the residuals that can be taken as evidence for varying reactivity of different adsorbed Fe^{II} species on these surfaces. Sensitivity analysis indicates that the calculated slopes are particularly sensitive to low-end values of $k_{red,surf}$ in each plot, where errors associated with subtracting the solution-reaction contribution, $k_{red,sol}$, is not negligible. That said, most of the reaction-order plots shown in Figure 9 do not markedly conflict with the assumed first-order kinetic dependence on total adsorbed Fe^{II}.

The log-log plots shown in Figure 9 for a few of the mineral phases (goethite, SiO$_2$ #1, #2) deviate somewhat from a slope of unity (as measured by the 95% confidence intervals). The calculated slope for goethite is 0.76 $\pm$ 0.08. The reduced slope could be explained by an increased degree of particle aggregation at higher S_{AL} and pH (conditions where Fe^{II} adsorption is greatest). If particle aggregation is significant, it can reduce the fraction of adsorbed Fe^{II} that is exposed to bulk solution and thus able to react with dissolved oxamyl. Aggregation of goethite particles at high S_{AL} could also help explain the deviation of the model predictions from experimental observations under these conditions (Fig. 5C, lower panel). If particles begin to aggregate at high S_{AL}, increases in [Fe^{II}]$_{ads}$ are counteracted to some extent by increases in the degree of particle aggregation. As a result, the concentration of "reactive" adsorbed Fe^{II} becomes lower than total [Fe^{II}]$_{ads}$. It then follows that further increases in S_{AL} have less of an effect on k_{red} than on [Fe^{II}]$_{ads}$. It is also worth noting that TEM characterization of the goethite particles shows a high degree of particle aggregation, but it is unclear whether this same mode of aggregation occurs under conditions examined in this study, or if it is simply an artifact of the TEM sample preparation procedure.

The log-log plots for SiO$_2$ #1 and #2 exhibit slopes that are somewhat greater than unity. The most likely explanation for this observation is that [Fe^{II}]$_{ads}$ is poorly defined in the SiO$_2$ suspensions. Fe^{II} adsorption onto SiO$_2$ surfaces is extremely weak and difficult to measure accurately under conditions used in kinetic experiments. As noted in section 3.4, the extent of Fe^{II} adsorption was estimated by linear extrapolation from adsorption measurements in 50 g L^{-1} suspensions of each SiO$_2$ mineral. These estimates assume that the extent of Fe^{II} adsorption increases linearly with increasing S_{AL}. Even small deviations from the assumed linear dependence could then explain the increased slopes observed in Figures 9J to 9K.

Kinetic trends shown in Figures 5 to 6 also support our second assumption that the kinetic contribution of reactions involving adsorbed oxamyl is negligible and can be ignored in most cases (i.e., the last three terms in Eqn. 6 are much smaller than the first three terms). Because the extent of oxamyl adsorption is low in all of our experiments (<5% of total oxamyl added to suspensions) we can assume that the concentration of adsorbed oxamyl exhibits a linear dependence on S_{AL}. If the reactivity of *adsorbed oxamyl* with adsorbed Fe^{II} is much greater than the reactivity of *dissolved oxamyl* with adsorbed Fe^{II} (by orders of magnitude), and if we assume that oxamyl
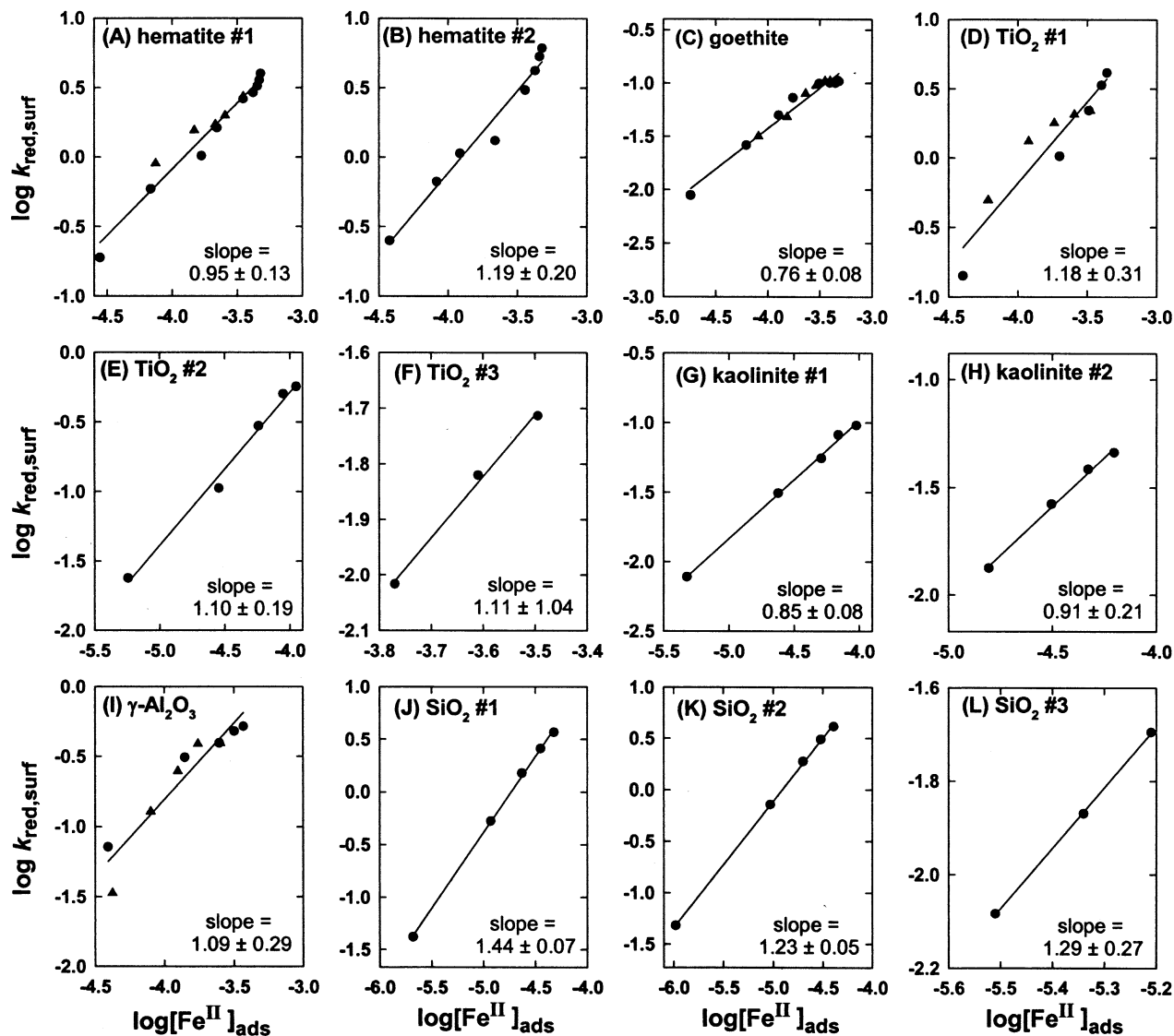
Fig. 9. Reaction-order plot for adsorbed Fe^{II}. $k_{red,surf}$ represents the surface-catalyzed contribution to k_{red}. Data from varied-S_{AL} experiments (●) and data from varied-pH experiments (▲). Lines indicate linear regression, and slopes indicate observed reaction order with respect to total adsorbed Fe^{II}. Uncertainty represents 95% confidence limit. When measured Fe^{II} adsorption is low (<5% of total Fe^{II}), $[Fe^{II}]_{ads}$ is calculated by linear extrapolation from measurements at higher S_{AL} (measurement error ~5%).

adsorption/desorption and surface diffusion processes are fast relative to the reaction with Fe^{II}, then we would expect overall kinetics (as measured by k_{red}) to exhibit a second-order dependence on S_{AL} when $[Fe^{II}]_{ads} \ll [Fe^{II}]_{tot}$ (due to the expected first-order dependence for both $[oxamyl]_{ads}$ and $[Fe^{II}]_{ads}$ under these conditions) and a first-order dependence on S_{AL} when $[Fe^{II}]_{ads}$ approaches $[Fe^{II}]_{tot}$ (due to an expected first-order dependence for $[oxamyl]_{ads}$ and near zero-order dependence for $[Fe^{II}]_{ads}$ under these conditions). In contrast to this, overall kinetics exhibit a near first-order dependence on S_{AL} when the extent of Fe^{II} adsorption is low, and less than first-order dependence on S_{AL} when $[Fe^{II}]_{ads}$ approaches $[Fe^{II}]_{tot}$. Furthermore, the addition of 5 and 20% methanol (v/v) to hematite #1

suspensions, which might be expected to alter the extent of oxamyl adsorption, has no effect on k_{red}. These results do not imply that the reactivity of adsorbed oxamyl with Fe^{II} is lower than the reactivity of dissolved oxamyl with Fe^{II}. Instead, they simply demonstrate that the contribution of adsorbed oxamyl to overall reaction kinetics (last three terms in Eqn. 6) is minimal, thus validating our second assumption.

It should also be mentioned than an alternative explanation for the increased slopes in the log-log plots calculated for SiO_2 #1 and #2 (Figs. 9J–9K) is the non-negligible contributions from one or more of the last three terms in Eqn. 6 (i.e., reactions involving adsorbed oxamyl molecules reacting with dissolved and adsorbed Fe^{II} species).

3.8. Comparison of Mineral Surfaces

The k_3 values derived from model fits vary considerably from one mineral phase to another, ranging from 5.99×10^1 $m^{-1} h^{-1}$ for TiO_2 #3 to $9.76 \times 10^4 m^{-1} h^{-1}$ for SiO_2 #2. This corresponds to 6- and 10,000-fold higher reactivity than Fe^{2+}_{aq}, respectively. For the surfaces examined, k_3 decreases in the following order: SiO_2 #2 > SiO_2 #1 ≫ hematite #2 > TiO_2 #1 > hematite #1 > TiO_2 #2 > SiO_2 #3 > γ-Al_2O_3 > kaolinite #1 > kaolinite #2 > goethite ≫ TiO_2 #3. It should be kept in mind, however, that the overall catalytic effect of a given surface is equal to the product of k_3 times $[Fe^{II}]_{ads}$. For example, even though k_3 obtained for the two synthetic SiO_2 surfaces are by far the highest, ~1 order of magnitude > k_3 obtained for the TiO_2 #1 and the two hematite surfaces, overall catalysis of oxamyl reduction is similar for all five surfaces because Fe^{II} adsorbs to a much greater extent on TiO_2 #1 and hematite surfaces.

In addition to variations in the reactivity of Fe^{II} adsorbed on (hydr)oxides of different metals, our findings indicate large variations in the reactivity of Fe^{II} adsorbed on (hydr)oxides composed of the same metal. Therefore, the reactivity of adsorbed Fe^{II} cannot be interpreted simply based on the identity of the metal that comprises the adsorbing mineral surface. We speculate that this is the rule, rather than the exception, for reactions involving mineral surfaces. Unfortunately, though, investigations are often limited to a small number of mineral surfaces, and too frequently generalizations are made about the reactivity or catalytic activity of entire classes of minerals (e.g., TiO_2) based upon results obtained with a single mineral preparation (e.g., TiO_2 type P-25 supplied by Degussa).

Our results indicate that Fe^{II} adsorbed on two different hematite surfaces exhibits similar reactivity with oxamyl, while Fe^{II} adsorbed on goethite appears significantly less reactive. This is in contrast to results of Buerge and Hug (1999) for the reduction of Cr^{VI}. They report similar reactivity for Fe^{II} adsorbed on goethite and lepidocrocite (γ-FeOOH). Tamura et al. (1980) also report that Fe^{II} adsorbed onto goethite, lepidocrocite, and akaganéite (β-FeOOH) exhibit similar reactivity with O_2. However, they also report that Fe^{II} adsorbed onto amorphous Fe^{III} (hydr)oxide is significantly more reactive towards O_2 than Fe^{II} adsorbed onto the three crystalline FeOOH surfaces.

We also found that k_3 varies considerably among the three TiO_2 surfaces, and k_3 values are much higher for two synthetic amorphous SiO_2 surfaces (#1, #2) than for SiO_2 #3, a naturally occurring quartz silica. Finally, k_3 is similar for both kaolinite surfaces (slightly higher for the poorly-crystalline form), and k_3 for both of these naturally-occurring aluminosilicates are slightly < k_3 for γ-Al_2O_3 and SiO_2 #3.

3.9. Interpreting Differences in k_3

Differences in the reactivity of Fe^{II} adsorbed on different mineral surfaces may be explained by several factors including (1) the crystal structure, (2) the identity of Fe^{II} complexes that predominate on a given surface, (3) the thermodynamics of the Fe^{III}/Fe^{II} redox couple, (4) the thermodynamics and kinetics of Fe^{II}-oxamyl bond formation, and (5) associated geometric or steric factors.

The chemistry of exposed surface functional groups is directly dependent upon the underlying crystal structure. The geometric arrangement of oxygen donor ligands and surface metal ions may be different for different crystal faces of the same mineral particle (e.g., (110) vs. (001) faces), and the interaction between Fe^{II} and surface functional groups may vary considerably from one crystal face to another. Consequently Fe^{II} reactivity may be significantly influenced by which crystal face it adsorbs onto. It follows that if Fe^{II} adsorption occurs on multiple crystal faces of the same mineral, the overall observed reactivity will be a function of the distribution of adsorbed Fe^{II} ions among crystal faces and the reactivity of Fe^{II} adsorbed on each crystal face of the mineral. One possible reason, then, for the variation in reactivity observed for different suspensions of the same mineral (e.g., TiO_2 surfaces) is that Fe^{II} reactivity varies significantly among crystal faces, and the predominant crystal face where Fe^{II} adsorption occurs varies among the minerals compared.

As mentioned already, total adsorbed Fe^{II} represents an ensemble of individual surface complexes that differ in several ways, including the dissolved metal species that adsorb (e.g., Fe^{2+}_{aq}, $FeOH^+_{aq}$), the mode of surface complexation (e.g., monodentate-mononuclear, bidentate-mononuclear, bidentate-binuclear), and the location on the surface where adsorption occurs (e.g., terrace, edge). It is likely that the reactivity of individual Fe^{II} surface complexes with oxamyl differs, just as the reactivity of dissolved Fe^{II} complexes differs (Strathmann and Stone, 2002a, 2002b). If different species predominate on different surfaces, then it follows that k_3 might be significantly affected. For example, if $(\equiv S-O)_2$-Fe^o is a more reactive surface complex than $\equiv S-O-Fe^+$, then the large difference in k_3 observed among the iron (hydr)oxides could be accounted for by a predominance of the former on hematite surfaces and the latter on goethite surfaces.

In homogeneous solutions, we found that the reactivity of different Fe^{II}-ligand complexes (FeL) with oxamyl is related to one-electron reduction potentials (E_H^o) of corresponding Fe^{III}/Fe^{II} redox couples ($Fe^{III}L + e^- = Fe^{II}L$) (Strathmann and Stone, 2002b). It follows that the reactivity of Fe^{II} surface complexes with oxamyl might also be related to E_H^o of the corresponding adsorbed redox couples ($Fe^{III}_{ads} + e^- = Fe^{II}_{ads}$).

Unfortunately, reliable values of E_H^o are not available for adsorbed Fe^{III}/Fe^{II} redox couples. Some studies have estimated E_H^o values for adsorbed Fe^{III}/Fe^{II} redox couples from extrapolation of linear free energy relationships (LFER) developed for dissolved Fe^{III}/Fe^{II} redox couples (Wehrli et al., 1989b uerge and Hug, 1999):

$$\log k_i = m E_H^o + b \quad (11)$$

where m and b are the slope and intercept of the LFER, respectively. If we assume that the LFER for oxamyl reduction by dissolved Fe^{II} species ($m = 6.27$ and $b = 6.16$) (Strathmann and Stone, 2002b) applies to adsorbed Fe^{II} species as well, then we can estimate E_H^o for adsorbed Fe^{III}/Fe^{II} redox couples by inserting the values of k_3 from Table 2 into Eqn. 11. The resulting LFER estimates of E_H^o for adsorbed Fe^{III}/Fe^{II} range from +0.22 to +0.66 V (Fig. 10). These values lie between E_H^o for $Fe^{3+}_{aq}/Fe^{2+}_{aq}$ (+0.77 V) and E_H^o for $Fe(OH)_2^+_{aq}$/
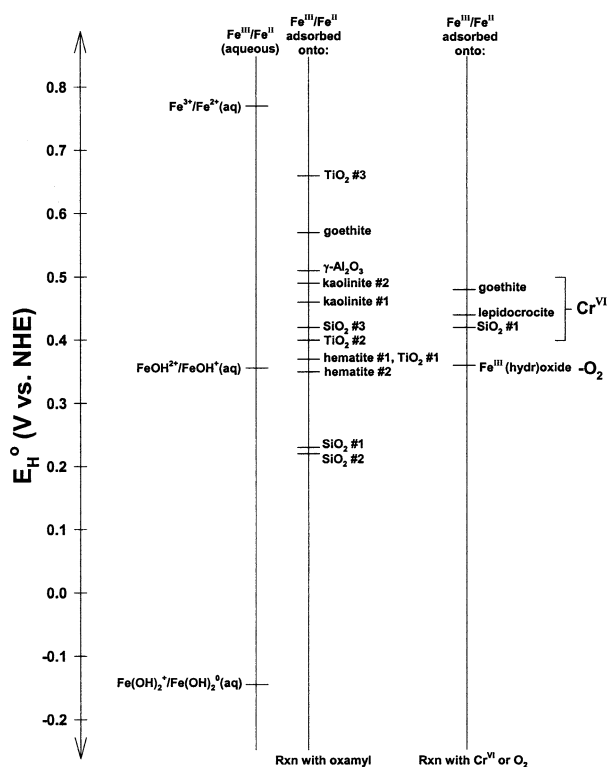
Fig. 10. Estimates of $E_H{}^o$ for adsorbed Fe^{III}/Fe^{II} redox couples obtained by extrapolation from the LFER reported for dissolved Fe^{II} species reacting with oxamyl (Strathmann and Stone, 2002b), Cr^{VI} (Buerge and Hug, 1999), and O_2 (Wehrli et al., 1989). Values of $E_H{}^o$ for dissolved species obtained as described previously (Strathmann and Stone, 2002a).

$Fe(OH)_2{}^o{}_{aq}$ (-0.145 V). Figure 10 also shows $E_H{}^o$ values estimated from a LFER for Cr^{VI} reduction (Buerge and Hug, 1999) and O_2 reduction (Wehrli et al., 1989). It is particularly useful to compare the $E_H{}^o$ values for Fe^{III}/Fe^{II} adsorbed on SiO_2 #1, because this surface is used in our study as well as the work of Buerge and Hug (1999). $E_H{}^o$ estimated from oxamyl kinetic data ($+0.23$ V) is significantly lower than the value estimated from Cr^{VI} kinetic data ($+0.42$ V). Likewise, $E_H{}^o$ for Fe^{III}/Fe^{II} adsorbed on goethite surfaces do not compare favorably ($+0.57$ V from oxamyl reduction; $+0.48$ V from Cr^{VI} reduction). This comparison is less useful, however, because the goethite preparations were different in each study. The discrepancy between $E_H{}^o$ values determined from oxamyl and Cr^{VI} kinetic data suggests that the utility of this sort of analysis is limited. This is not surprising given that total adsorbed Fe^{II} represents an ensemble of different surface-complexed species, and each species is likely to have a unique $E_H{}^o$ that depends on several factors, including (1) which Fe^{II} species is adsorbed (e.g., Fe^{2+}, $FeOH^+$), (2) the mode of bonding (e.g., monodentate-mononuclear, bidentate-binuclear), and (3) the σ- and π-donor characteristics of the surface-bound oxygen ligands at a particular location on the surface. Furthermore, surface catalysis of redox reactions involving Fe^{II} is likely to involve more than just changes in $E_H{}^o$. Therefore, using solution-phase LFERs (for reduction of oxamyl or any other oxidant) for predicting $E_H{}^o$ of adsorbed Fe^{III}/Fe^{II} redox couples is questionable.

Results from our work with solution-phase ligands indirectly suggest that the formation of weak inner-sphere Fe^{II}-oxamyl precursor complexes leads to elevated rates of OCP reduction, and that bidentate coordination in the precursor complex enhances reaction kinetics more than monodentate coordination (Strathmann and Stone, 2002b). Oxamyl coordination to adsorbed Fe^{II} species could be important as well, and it is possible that some surfaces favor bidentate Fe^{II}-oxamyl coordination, while other surfaces favor monodentate coordination. For example, one could imagine that bidentate Fe^{II}-oxamyl coordination might be inhibited on a particular surface if neighboring surface sites are located such that they create unfavorable electronic or steric interactions with a bidentate-coordinated oxamyl molecule. Unfortunately, we are unable to characterize either the oxamyl complexes with adsorbed Fe^{II}, or the neighboring surface site population surrounding the Fe^{II} surface complexes.

Lastly, values of k_3 may be affected by geometric factors. For example, some Fe^{II} adsorption sites, such as those on the bottom of small pits present on mineral terraces, will not be readily accessible by the large oxamyl molecule. Likewise, some mineral phases may aggregate more than others, and a significant fraction of adsorbed Fe^{II} could end up in the aggregate interior where it is physically unavailable for reaction with oxamyl. Hence, even if the inherent reactivity of adsorbed Fe^{II} is similar for all surfaces, geometric factors could lead to diminished values of k_3 for some heavily aggregated mineral suspensions.

Ultimately, our interpretation of the reactivity of Fe^{II} adsorbed on different surfaces is limited by our current understanding of the mineral-water interface on the molecular length scale. Surface chemical information on scales of a few bond lengths or less is most relevant for assessing chemical reactivity. This would include information on the spatial distribution of adsorption sites, characteristics of different types of adsorption sites (e.g., terrace, edge, kink), metal-to-metal distances in the near-surface structure, and structures of different Fe^{II} surface complexes, as well as information on the effects of each of these properties on the coordination chemistry of Fe^{II}. Several groups are currently working to improve our understanding of the mineral-water interface on this scale (Hiemstra et al., 1989; Junta-Rosso et al., 1997; Koretsky et al., 1998; Brown et al., 1999; Rietra et al., 1999).

3.10. Comparison of Related Oxime Carbamates

A series of reactions was carried out to compare the effects of mineral surfaces on the reactions between Fe^{II} and three structurally related OCPs, oxamyl, methomyl, and aldicarb. Figure 11 compares measured first-order rate constants (k_{red}) for the three OCPs in suspensions where the identity of the mineral phase, S_{AL}, pH (7.4), $[Fe^{II}]_{tot}$, and concentrations of all other pertinent chemical species are the same. For each mineral suspension, k_{red} decreases in the order: methomyl > oxamyl > aldicarb. This is the same trend reported for solutions containing dissolved organic and inorganic ligands (Strathmann and Stone, 2002a, 2002b). Both plots exhibit a linear correlation with a slope close to unity, indicating that mineral surfaces affect the reduction of all three pesticides in the same fashion. This result implies that if we were to determine bimolecular
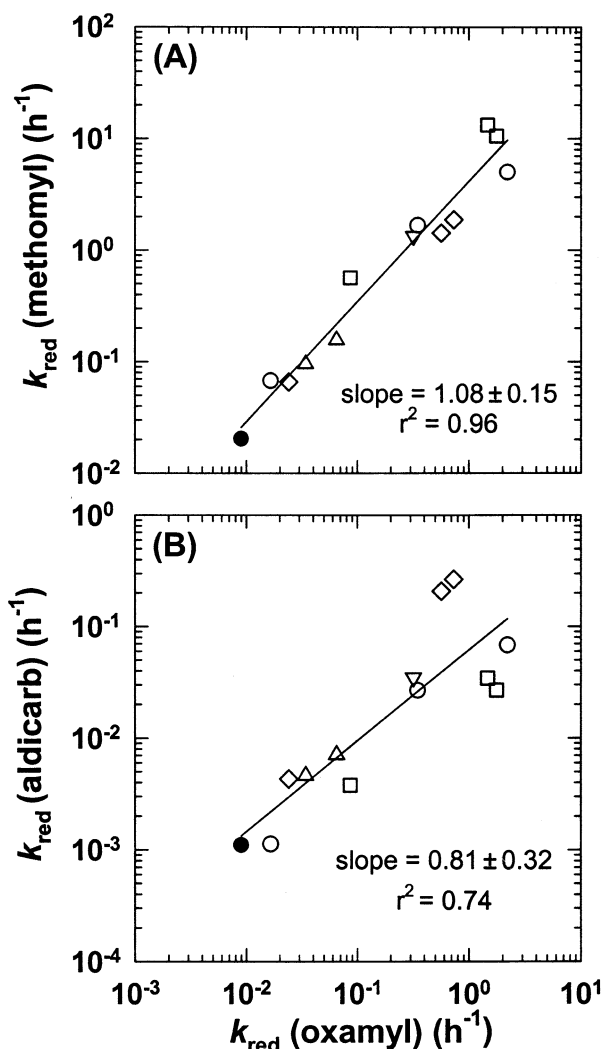
Figure 11. Comparison of measured k_{red} for oxamyl with (A) measured k_{red} for methomyl, and (B) measured k_{red} for aldicarb in selected mineral suspensions of equivalent composition. Symbols indicate homogeneous solution (●), and suspensions of iron (hydr)oxides (□), silicon dioxides (○), titanium dioxides (◇), γ-Al_2O_3 (▽), and kaolinites (△). Reaction conditions: 0.5 mmol/L total Fe^{II}, 25 μmol/L OCP, pH 7.4 (25 mmol/L MOPS), 100 mmol/L NaCl, and 25°C. Suspensions contained the following mass loadings: 1 g/L (goethite, hematite #1, #2), 1.25 g/L (SiO_2 #2), and 5 g/L (all other solids). Lines indicate linear regression, and uncertainties represent 95% confidence limits.

rate constants for methomyl or aldicarb reacting with adsorbed Fe^{II} (k_3; this would require a large number of experiments), we would expect approximately the same pattern of values determined for oxamyl (Table 2). For example, for all three OCPs we expect Fe^{II} adsorbed on hematite #1 to be ~800-fold more reactive than Fe^{2+}_{aq}.

4. CONCLUSIONS

The results of this study suggest that Fe^{II} adsorbed on mineral surfaces found in subsurface environments may be an effective reductant for OCPs and related agrochemicals. Kinetic trends indicate that adsorbed Fe^{II} is significantly more reactive with these compounds than Fe^{2+}_{aq}, and results support a hypothesis that catalysis occurs as the result of Fe^{II} complexation by surface-bound oxygen donor ligands. This follows from our prior work that demonstrates that Fe^{II} reactivity with OCPs is markedly affected upon complexation by dissolved inorganic and organic ligands.

Anoxic and suboxic environments are often characterized by high Fe^{II} concentrations, the result of the ubiquitous presence of Fe^{III}-reducing bacteria, and it is likely that a significant fraction of the Fe^{II} in soils and aquifers is adsorbed onto (hydr)oxide and aluminosilicate particles or surface coatings. Our findings indicate that OCPs will rapidly degrade in these systems.

Surface-catalyzed reduction of OCPs is also significantly faster than base-catalyzed elimination, the predominant degradation pathway observed in oxic soils and groundwater (Bromilow et al., 1980; Miles and Delfino, 1985; Lightfoot et al., 1987; Warren et al., 2000). This suggests that these compounds will degrade more rapidly in reducing environments than in oxygenated environments.

Results from this study also improve our understanding of Fe^{II} reactivity with organic oxidants in aqueous environments. Most studies on the reactivity of Fe^{II} with organic compounds have been limited to a small number of compounds, most notably nitrobenzenes and halogenated alkanes. Our work with OCPs complements these studies and expands our overall understanding of the organic functional groups that are susceptible to reduction by Fe^{II}. We suspect that other classes of widely used synthetic chemicals are also susceptible to reduction by Fe^{II}, especially in heterogeneous systems containing numerous catalytic mineral surfaces. However, because these compounds lack halogenated or nitroaromatic functional groups in their structures, few studies have been directed at assessing their reactivity with Fe^{II} and other environmentally relevant reducing agents.

Finally, OCPs provide us with another set of compounds for probing redox processes in reducing environments. Results from this work and prior studies in this series indicate that the reactivity of OCPs is influenced by factors such as the thermodynamics of the Fe^{III}/Fe^{II} redox couple, as well as the number of coordination positions occupied by complexing ligands. By comparing the relative reactivity of multiple classes of oxidants (e.g., OCPs vs. nitrobenzenes vs. Cr^{VI}) observed in model systems (e.g., Fe^{II} adsorbed on a series of mineral surfaces) with the relative reactivity observed in complex soil systems, we may improve our understanding of the relevant catalytic constituents present in natural environments.

REFERENCES

Amonette J. E., Workman D. J., Kennedy D. W., Fruchter J. S., and Gorby Y. A. (2000) Dechlorination of carbon tetrachloride by Fe(II) associated with goethite. *Environ. Sci. Technol.* **34,** 4606–4613.

Bank S. and Tyrrell R. J. (1984) Kinetics and mechanism of alkaline and acidic hydrolysis of aldicarb. *J. Agric. Food Chem.* **32,** 1223–1232.

Bromilow R. H., Baker R. J., Freeman M. A. H., and Görög K. (1980) The Degradation of aldicarb and oxamyl in soil. *Pestic. Sci.* **11,** 371–378.

Bromilow R. H., Briggs G. G., Williams M. R., Smelt J. H., Tuinstra L. G. M. T., and Traag W. A. (1986) The role of ferrous ions in the rapid degradation of oxamyl, methomyl and aldicarb in anaerobic soils. *Pestic. Sci.* **17,** 535–547.

Brown G. E., Henrich V. E., Casey W. H., Clark D. L., Eggleston C., Felmy A., Goodman D. W., Gratzel M., Maciel G., McCarthy M. I., Nealson K. H., Sverjensky D. A., Toney M. F., and Zachara J. M. (1999) Metal oxide surfaces and their interactions with aqueous solutions and microbial organisms. *Chem. Rev.* **99,** 77–174.

Bruemmer G. W., Gerth J., and Tiller K. G. (1988) Reaction kinetics of the adsorption and desorption of nickel, zinc and cadmium by goethite. I. Adsorption and diffusion of metals. *J. Soil. Sci.* **39,** 37–52.

Buerge I. J. and Hug S. J. (1998) Influence of organic ligands on chromium(VI) reduction by iron(II). *Environ. Sci. Technol.* **32,** 2092–2099.

Buerge I. J. and Hug S. J. (1999) Influence of mineral surfaces on chromium(VI) reduction by iron(II). *Environ. Sci. Technol.* **33,** 4285–4291.

Cervini-Silva J., Wu J., Larson R. A., and Stucki J. W. (2000) Transformation of. chloropicrin in the presence of iron-bearing clay minerals. *Environ. Sci. Technol.* **34,** 915–917.

Charlet L., Silvester E., and Liger E. (1998) N-compound reduction and actinide immobilisation in surficial fluids by Fe(II): The surface >Fe^{III}OFe^{II}OH^0 species as major reductant. *Chem. Geol.* **151,** 85–93.

Coughlin B. A. and Stone A. T. (1995) Nonreversible adsorption of divalent metal ions (Mn^{II}, Co^{II}, Ni^{II}, Cu^{II}, and Pb^{II}) onto goethite: Effects of acidification, Fe^{II} addition, and picolinic acid addition. *Environ. Sci. Technol.* **29,** 2445–2455.

Cui D. and Eriksen T. E. (1996) Reduction of pertechnetate by ferrous iron in solution: Influence of sorbed and precipitated Fe(II). *Environ. Sci. Technol.* **30,** 2259–2262.

Davies S. H. R. and Morgan J. J. (1989) Manganese(II) oxidation kinetics on metal oxide surfaces. *J. Colloid Interface Sci.* **129,** 63–77.

Dean G. M., Mellor S. J., Ward C. L., and Warren. R. L. (2000) Field collection, transport, and laboratory maintenance of saturated aerobic and anaerobic subsoils. Poster presented at the Third Society of Environmental Toxicology and Chemistry World Congress, Brighton, UK, May.

Deng B. and Stone A. T. (1996) Surface-catalyzed chromium(VI) reduction: The TiO$_2$-Cr^{VI}-mandelic acid system. *Environ. Sci. Technol.* **30,** 463–472.

Erbs M., Hansen H. C. B., and Olsen C. E. (1999) Reductive dechlorination of carbon tetrachloride using iron(II) iron(III) hydroxide sulfate (green rust). *Environ. Sci. Technol.* **33,** 307–311.

Feitknecht W. and Schindler P. (1963) Löslichkeitskonstanten von Metalloxiden, -Hydroxiden, und -Hydroxidsalzen in Wässrigen Lösungen. *Pure Appl. Chem.* **6,** 125–199.

Fridrikhsberg D. A. (1986) *A Course in Colloid Chemistry.* Mir Publishers, Moscow, Russia.

Hale D. D., Rogers J. E., and Wiegel J. (1991) Environmental factors correlated to dichlorophenol dechlorination in anoxic fresh waters. *Environ. Toxicol. Chem.* **10,** 1255–1265.

Hayes K., Redden G., Ela W., and Leckie J. O. (1991) Surface complexation models—An evaluation of model parameter-estimation using FITEQL and oxide mineral titration data. *J. Colloid Interface Sci.* **142,** 448–469.

Hegarty A. F. and Frost L. N. (1973) Elimination-addition mechanism for the hydrolysis of carbamates. Trapping of an isocyanate intermediate by an *o*-amino-group. *J. Chem Soc., Perkin Trans.* **2,** 1719–1728.

Heijman C. G., Holliger C., Glaus M. A., Schwarzenbach R. P., and Zeyer J. (1993) Abiotic reduction of 4-chloronitrobenzene to 4-chloronitroaniline in a dissimilatory iron-reducing enrichment culture. *Appl. Environ. Microbiol.* **59,** 4350–4353.

Heijman C. G., Grieder E., Holliger C., and Schwarzenbach R. P. (1995) Reduction of nitroaromatic compounds coupled to microbial iron reduction in laboratory aquifer columns. *Environ. Sci. Technol.* **29,** 775–783.

Hering J. G. and Stumm W. (1990) Oxidative and reductive dissolution of minerals. In *Mineral-Water Interface Geochemistry* (eds. M. F. Hochella and A. F. White), *Rev. Mineral.* **23,** 427–465. Mineralogical Society of America, Washington, DC.

Hiemstra T., van Riemsdijk W. H., and Bolt G. H. (1989) Multisite proton adsorption modeling at the solid-solution interface of (hydr)oxides—A new approach. 1. Model description and evaluation of intrinsic reaction constants. *J. Colloid Interface Sci.* **133,** 91–104.

Huang C.-H (1997) *Hydrolysis of Amide, Carbamate, Hydrazide and Sulfonylurea Agrochemicals: Catalysis and Inhibition by Dissolved Metal Ions, Metal Ion-Ligand Complexes and Hydrous Oxide Surfaces.* Ph.D. dissertation, Johns Hopkins University, Baltimore, MD.

Jeon B. H. Dempsey B. A., Burgos W. D., and Royer R. A. (2001) Reactions of ferrous iron with hematite. *Colloids Surf. A* **191,** 41–55.

Junta-Rosso J. L., Hochella M. F. Jr., and Rimstidt J. D. (1997) Linking microscopic and macroscopic data for heterogeneous reactions illustrated by the oxidation of manganese(II) at mineral surfaces. *Geochim. Cosmochim. Acta* **61,** 149–159.

King D. W. (1998) Role of carbonate speciation on the oxidation rate of Fe(II) in aquatic systems. *Environ. Sci. Technol.* **32,** 2997–3003.

King D. W. and Farlow R. (2000) Role of carbonate speciation on the oxidation of Fe(II) by H$_2$O$_2$. *Mar. Chem.* **70,** 201–209.

Klausen J., Tröber S. P., Haderlein S. B., and Schwarzenbach R. P. (1995) Reduction of substituted nitrobenzenes by Fe(II) in aqueous mineral suspensions. *Environ. Sci. Technol.* **29,** 2396–2404.

Koretsky C. M., Sverjensky D. M., and Sahai N. (1998) A model of surface site types on oxide and silicate minerals based on crystal chemistry: Implications for site types and densities, multi-site adsorption, surface infrared spectroscopy, and dissolution kinetics. *Am. J. Sci.* **298,** 349–438.

Kummert R. and Stumm W. (1980) The surface complexation of organic acids on hydrous γ-Al$_2$O$_3$. *J. Colloid Interface Sci.* **75,** 373–385.

Larson R. A. and Weber E. J. (1994) *Reaction Mechanisms in Environmental Organic Chemistry.* Lewis Publishers, Boca Raton, FL.

Liang L. (1988) *Effect of Surface Chemistry on Kinetics of Coagulation of Submicron Iron Oxide Particles (α-Fe$_2$O$_3$) in Water.* Ph.D. dissertation, California Institute of Technology, Pasadena.

Liger E., Charlet L., and VanCappellen P. (1999) Surface catalysis of uranium(VI) reduction by iron(II). *Geochim. Cosmochim. Acta* **63,** 2939–2956.

Lightfoot E. N., Thorne P. S., Jones R. L., Hansen J. L., and Romine R. R. (1987) Laboratory studies on mechanisms for the degradation of aldicarb, aldicarb sulfoxide and aldicarb sulfone. *Environ. Toxicol. Chem.* **6,** 377–394.

Lovley D. R. and Phillips E. J. P. (1988) Novel mode of microbial energy metabolism: Organic carbon oxidation coupled to dissimilatory reduction of iron or manganese. *Appl. Environ. Microbiol.* **54,** 1472–1480.

Martell A. E., Smith R. M., and Motekaitis R. J. (1997) *Critically Selected Stability Constants of Metal Complexes Database.* U.S. Department of Commerce, National Institute of Standards and Technology.

Miles C. J. and Delfino J. J. (1985) Fate of aldicarb, aldicarb sulfoxide, and aldicarb sulfone in Floridan groundwater. *J. Agric. Food Chem.* **33,** 455–460.

Millero F. J., Sotolongo S., Stade D. J., and Vega C. A. (1991) Effect of ionic interactions on the oxidation of Fe(II) with H$_2$O$_2$ in aqueous solutions. *J. Solution Chem.* **20,** 1079–1092.

Nowack B., Lützenkirchen J., Behra P., and Sigg L. (1996) Modeling the adsorption of metal-EDTA complexes onto oxides. *Environ. Sci. Technol.* **30,** 2397–2405.

Park J. S. B., Wood P. M., Davies M. J., Gilbert B. C., and Whitwood A. C. (1997) A kinetic and ESR investigation of iron(II) oxalate oxidation by hydrogen peroxide and dioxygen as a source of hydroxyl radicals. *Free Rad. Res.* **27,** 447–458.

Pec her K., Haderlein S. B., and Schwarzenbach R. P. (2002) Reduction of polyhalogenated methanes by surface-bound Fe(II) in aqueous s uspensions of iron oxides. *Environ. Sci. Technol.* **36,** 1734–1741.

Peijnenburg W. J. G. M., Hart M. J. T., Hollander H. A. D., Meent D. V. D., Verboom H. H., and Wolfe N. L. (1992) Reductive transformations of halogenated aromatic hydrocarbons in anaerobic water-sediment systems: Kinetics, mechanisms and products. *Environ. Toxicol. Chem.* **11,** 289–300.

Penn R. L., Oskam G., Strathmann T. J., Searson P. C., Stone A. T., and Veblen D. R. (2001) Epitaxial assembly in aged colloids. *J. Phys Chem. B* **105,** 2177–2182.

Postma D., Boesen C., Kristiansen H., and Larsen F. (1991) Nitrate reduction in an unconfined sandy aquifer: Water chemistry, reduction processes, and geochemical modeling. *Wat. Resour. Res.* **27,** 2027–2045.

Rietra R. P. J. J., Hiemstra T., and van Riemsdijk W. H. (1999) The relationship between molecular structure and ion adsorption on variable charge minerals. *Geochim. Cosmochim. Acta* **63,** 3009–3015.

Rügge K., Hofstetter T. B., Haderlein S. B., Bjerg P. L., Knudsen S., Zraunig C., Mosbæk H., and Christensen T. H. (1998) Characterization of predominant reductants in an anaerobic leachate-contaminated aquifer by nitroaromatic probe compounds. *Environ. Sci. Technol.* **32,** 23–31.

Schultz C. A. and Gundl T. J. (2000) pH dependence on reduction rate of 4-Cl-nitrobenzene by Fe(II)/montmorillonite systems. *Environ. Sci. Technol.* **34,** 3641–3648.

Schwarzenbach R. P., Stierli R., Lanz K., and Zeyer J. (1990) Quinone and iron porphyrin mediated reduction of nitroaromatic compounds in homogenous aqueous solution. *Environ. Sci. Technol.* **24,** 1566–1574.

Stone A. T., Godtfredsen K. L., and Deng B. (1994) Sources and reactivity of reductants encountered in aquatic environments. In *Chemistry of Aquatic Systems: Local and Global Perspectives* (eds. G. Bidoglio and W. Stumm), pp. 337–374. Kluwer, Dordrecht, the Netherlands.

Stookey L. L. (1970) Ferrozine—A new spectrophotometric reagent for iron. *Anal. Chem.* **42,** 779–781.

Strathmann T. J. (2001) *Metal Ion-Facilitated Reduction of Oxime Carbamate Pesticides: Influence of Metal Ion Speciation.* Ph.D. dissertation, Johns Hopkins University, Baltimore, MD.

Strathmann T. J. and Stone A. T. (2001) Reduction of the carbamate pesticides oxamyl and methomyl by dissolved Fe[II] and Cu[I]. *Environ. Sci. Technol.* **35,** 2461–2469.

Strathmann T. J. and Stone A. T. (2002a) Reduction of the pesticides oxamyl and methomyl by Fe[II]: Effect of pH and inorganic ligands. *Environ. Sci. Technol.* **36,** 653–661.

Strathmann T. J. and Stone A. T. (2002b) Reduction of oxamyl and related pesticides by Fe[II]: Influence of organic ligands and natural organic matter. *Environ. Sci. Technol.* **36,** 5172–5183.

Stumm W. (1992) *Chemistry of the Solid-Water Interface: Processes at the Mineral-Water and Particle-Water Interface in Natural Systems.* John Wiley, New York.

Stumm W. and Lee G. F. (1961) Oxygenation of ferrous iron. *Ind. Eng. Chem.* **53,** 143–146.

Sutheimer S. H., Maurice P. A., and Zhou Q. (1999) Dissolution of well and poorly crystallized kaolinites: Al speciation and effects of surface characteristics. *Am. Mineral.* **84,** 620–628.

Tamura H., Goto K., and Nagayama M. (1976) Effect of anions on the oxygenation of ferrous ion in neutral solutions. *J. Inorg. Nucl. Chem.* **38,** 113–117.

Tamura H., Kawamura S., and Hagayama M. (1980) Acceleration of the oxidation of Fe^{2+} ions by Fe(III)-oxyhydroxides. *Corros. Sci.* **20,** 963–971.

Tomizawa C. (1975) Degradation of organophosphorus pesticides in soils with special reference to unaerobic soil conditions. *Environ. Qual. Saf.* **4,** 117–127.

Torrents A. (1992) *Hydrolysis of Organic Esters at the Mineral/Water Interface.* Ph.D. dissertation, Johns Hopkins University, Baltimore, MD.

Vasudevan D. and Stone A. T. (1998) Adsorption of 4-nitrocatechol, 4-nitro-2-aminophenol, and 4-nitro-1,2-phenylenediamine at the metal (hydr)oxide/water interface: Effect of metal (hydr)oxide properties. *J. Colloid Interface Sci.* **202,** 1–19.

Vikesland P. J. and Valentine R. L. (2002) Iron-oxide surface catalyzed reduction of monochloramine by ferrous iron: Implications of oxide type and carbonate on reactivity. *Environ. Sci. Technol.* **36,** 512–519.

Wade R. S. and Castro C. E. (1973) Oxidation of iron(II) porphyrins by alkyl halides. *J. Am. Chem. Soc.* **95,** 226–230.

Walters-Echols G. and Lichtenstein E. P. (1977) Microbial reduction of phorate sulfoxide to phorate in a soil-lake mud-water microcosm. *J. Econ. Entomol.* **70,** 505–509.

Warren R. L., Dean G. M., Mellor S. J., and Ward. C. L. (2000) Degradation of oxamyl in saturated subsoils. Poster presented at the Third Society of Environmental Toxicology and Chemistry World Congress, Brighton, UK, May.

Wehrli B., Sulzberger B., and Stumm W. (1989) Redox processes catalyzed by hydrous oxide surfaces. *Chem. Geol.* **78,** 167–179.

Young J. R. (1982) *A Study of the Adsorption of Ni(II) Onto an Amorphous Silica Surface by Chemical and NMR Methods.* Ph.D. dissertation, California Institute of Technology, Pasadena.

Zhang L., Larson R. A., Stucki J. W., and Kostka J. E. (Personal Communication).